

**University  
of Dundee**

**Control Design of a Surgical  
Robot Actuated  
by Cable Including Friction  
Problems and  
Inverse Kinematics**

**Ivan Kossko**

**Submitted for the degree of  
BEng (Hons) Biomedical Engineering**

**Supervisor: Luigi Manfredi**


**School of Science and Engineering**

**University of Dundee**

**April 2024**

## DECLARATION

I, Ivan Kossko, student of the School of Science and Engineering at the University of Dundee, hereby declare that I am the sole author of this thesis titled ‘Control Design of a Surgical Robot Actuated by Cable Including Friction Problems and Inverse Kinematics’. All work, unless otherwise specified, is my own and has not been previously accepted for a higher degree.

Signed:   
(Ivan Kossko)

Date: 21/04/25

## **ACKNOWLEDGEMENTS**

I would like to express my sincere gratitude to my supervisor, Dr Luigi Manfredi, for his invaluable guidance throughout this project during numerous meetings and discussions. Thank you to Zijian Liu for helping with manufacturing expertise as well as Calum MacRobert for help during 3D printing.

Finally, my deepest thanks to Mum and Dad for their unwavering encouragement and support.

## **ABSTRACT**

This project presents the design, simulation, and partial fabrication of a soft robotic manipulator actuated by cables, specifically developed for minimally invasive surgical applications. The project addresses key challenges associated with cable-driven soft robotics, notably frictional losses and the complexity of inverse kinematics in flexible, continuum structures. the project successfully demonstrated the feasibility of simulating and partially realising a multi-degree of freedom cable-actuated soft robotic manipulator. The findings underscore the importance of incorporating friction-aware modelling, robust control frameworks, and improved internal channel design to enhance performance.

## TABLE OF CONTENTS

DECLARATION.....	i
ACKNOWLEDGEMENTS .....	ii
ABSTRACT.....	iii
TABLE OF CONTENTS .....	iv
LIST OF FIGURES.....	vii
LIST OF EQUATIONS.....	ix
ABBREVIATIONS AND DEFINITIONS.....	xi
1 Introduction .....	1
2 Background .....	3
2.1 Overview of Robotic-Assisted Surgery .....	3
2.2 Soft Robotics in Surgical Applications .....	4
2.3 Cable-Driven Actuation Systems .....	5
2.4 Friction in Cable Actuated Robots .....	8
2.5 Inverse Kinematics in Surgical Robotics .....	9
2.6 Control Strategies for Soft Robotic Systems .....	12
2.7 Gap in Current Research .....	14
3 Methodology .....	16
3.1 Aims and Objectives .....	16
3.2 Initial Design.....	17

3.3	3-DOF Spring-Based Model (Proof of Concept) .....	18
3.4	Calculations.....	20
3.4.1	Geometric Construction of an Arc .....	20
3.4.2	Torque Due to Cable Offset.....	22
3.4.3	Frictional Effects in Cable-Driven Soft Robotics under Curvature .....	23
3.5	MATLAB Simulation.....	24
3.5.1	3 DoF Model .....	24
3.4.2	6 DoF Final Model .....	25
3.6	Mould Design and Fabrication of 6 DoF Model.....	28
4	Results .....	33
4.1	Software Simulation.....	33
4.1.1	3-DOF Arc Simulation (Proof of Concept).....	33
4.1.2	6-DOF Arc Simulation and Cable Mapping .....	34
4.2	Hardware Prototyping and Actuation.....	35
4.2.1	3-DOF Printed Model .....	35
4.2.2	Final 6-DOF Soft Robotic Limb .....	36
5	Discussion .....	39
5.1	Performance of the Simulation Environment.....	39
5.2	Hardware Performance and Limitations .....	40
5.3	Design and Fabrication Reflections .....	44
6	Conclusion .....	47

References .....	48
Appendix .....	52
Appendix A: Code Repository .....	52
Appendix B: Project Plan.....	53

## LIST OF FIGURES

Figure 1 - Motion analysis in non-restriction environment .....	4
Figure 2 - The complete cable-driven remotely actuated neurosurgical robotic system, MINIR-II .....	6
Figure 3 - Principle diagram of the 4-DoF surgical robot end-effector .....	7
Figure 4 - 3D model of the 4-DoF surgical robot end-effector. ....	7
Figure 5 - Segmentation representation model for multi-section flexible robots .....	11
Figure 6 - (1) Rigid Spine (2) Soft, flexible material (3) Full Concept Design.....	17
Figure 7 - 3D printable proof of concept backbone .....	18
Figure 8 - Proof of Concept model .....	18
Figure 9 - Proof of Concept Testing Setup.....	19
Figure 10 - Cable Routing in MATLAB Simulation.....	26
Figure 11 - Electronic Control Setup .....	27
Figure 12 - Mould Design.....	28
Figure 13 - (1) Mould Components After Printing (2) Fully Assembled Mould.....	29
Figure 14 - (1) Ecoflex 00-10 Packaging (2) Mixing Process of Both Parts of Ecoflex Mixture.....	30
Figure 15 - Vacuum Oven Air Removal.....	31
Figure 16 - Curing Inside Oven at 60° Celsius for 20 Minutes .....	31
Figure 17 - 6 DoF Prototype Mounted on Test Bench .....	32
Figure 18 - 3 DoF Simulation Output .....	33



Figure 19 - 6 DoF MATLAB Simulation Output.....	34
Figure 20 - Example Position Servo Angles and Spin Duration Instructions .....	35
Figure 21 - 3 DoF Proof of Concept in (1) Neutral Position (2) In Actuated Position ...	36
Figure 22 - Disassembled Parts of 6 DoF Model.....	37
Figure 23 - Mould after Vacuum and Oven Treatment .....	37
Figure 24 - Final 6 DoF Model Assembly on Test Bench.....	38
Figure 25 - Display of Irregular Deformation in Proof of Concept .....	40
Figure 26 - Actuation of Model Based on Simulation .....	41
Figure 27 - Maximum Curvature That Could be Mechanically Achieved with Current Model .....	43

## LIST OF EQUATIONS

$$d = \sqrt{(x_B - x_A)^2 + (y_B - y_A)^2 + (z_B - z_A)^2} \quad (1)$$

$$L = R\theta, \quad d = 2R\sin\left(\frac{\theta}{2}\right) \quad (2)$$

$$d = 2R\sin\left(\frac{L}{2R}\right) \quad (3)$$

$$M = \left(\frac{x_A+x_B}{2}, \frac{y_A+y_B}{2}, \frac{z_A+z_B}{2}\right) \quad (4)$$

$$h = \sqrt{R^2 - \left(\frac{d}{2}\right)^2} \quad (5)$$

$$\vec{u}_{\text{perp}} = \vec{u} - (\vec{u} \cdot \hat{v})\hat{v} \quad (6)$$

$$\vec{n} = \frac{\vec{u}_{\text{perp}}}{|\vec{u}_{\text{perp}}|} \quad (7)$$

$$\vec{n}_{\text{rot}} = \vec{n}\cos\phi + (\hat{v} \times \vec{n})\sin\phi + \hat{v}(\hat{v} \cdot \vec{n})(1 - \cos\phi) \quad (8)$$

$$C = M + h \cdot \vec{n}_{\text{rot}} \quad (9)$$

$$\vec{e}_1 = \frac{P_A - C}{|P_A - C|} \quad (10)$$

$$\vec{e}_2 = \frac{P_B - C - R\cos\theta \cdot \vec{e}_1}{R\sin\theta} \quad (11)$$

$$P(t) = C + R\cos t \cdot \vec{e}_1 + R\sin t \cdot \vec{e}_2, \quad t \in [0, \theta] \quad (12)$$

$$x = R\sin\theta \quad (13)$$

$$z = R(1 - \cos\theta) \quad (14)$$

$$\vec{r}_{\text{tip}} = (R\sin\theta, 0, R(1 - \cos\theta)) \quad (15)$$

$$\vec{r}_{\text{cable}} = (R\sin\theta + r_{\text{offset}}\cos\theta, 0, R(1 - \cos\theta) + r_{\text{offset}}\sin\theta) \quad (16)$$

$$\vec{F} = (0, 0, -F) \quad (17)$$

$$\vec{M} = \vec{r}_{\text{cable}} \times \vec{F} = (0, F(R\sin\theta + r_{\text{offset}}\cos\theta), 0) \quad (18)$$

$$d_{\text{eff}} = R\sin\theta + r_{\text{offset}}\cos\theta \quad (19)$$

$$M = F \cdot d_{\text{eff}} = F(R\sin\theta + r_{\text{offset}}\cos\theta) \quad (20)$$

$$T_2 = T_1 e^{\mu\theta} \quad (21)$$

$$\theta = \frac{L}{R} \quad (22)$$

## ABBREVIATIONS AND DEFINITIONS

The following table describes the significance of various abbreviations and acronyms used throughout the thesis. The page on which each one is defined or first used is also given.

Abbreviation	Definition	Page
IK	Inverse kinematics	4
TPU	Thermoplastic polyurethanes	5
DoF	Degrees of Freedom	6
PCC	Piecewise constant curvature	10
PDQ	Piecewise Dual Quaternion	10
PID	Proportional-integral-derivative	12
MPC	Model predictive control	13
FDM	Fused deposition modelling	18
PLA	Polylactic acid	18
PWM	Pulse-width modulation	26
GUI	Graphical user interface	33

# 1 Introduction

Biomedical engineering continuously seeks new approaches to enhance surgical outcomes for patients through the use and integration of robotic technologies. Robotic technologies hold significant potential in assisting surgeons and other medical professionals by reducing invasiveness and maximising surgical precision. Within this context, soft robotics has emerged as a transformative subfield, offering unparalleled adaptability to anatomical variations as well as improving safety by reducing the risk of unintentional damage to surrounding tissue. However, current robotic systems integrating soft actuators often encounter challenges ranging from precise motion control, complex inverse kinematics and when using cables, slight inaccuracies from friction caused by cable actuation. These challenges can diminish their operational effectiveness and reliability, underscoring the need for development of advanced control and modelling strategies whilst simultaneously keeping the user interface as intuitive as possible.

Cable actuated systems are widely used in surgical robotics due to their compact structure and ability to transmit forces effectively in constrained environments. However, their mechanical design introduces frictional forces at various points, which can reduce the precision of movement and complicate control strategies resulting in less responsive control, or the need for powerful computing power. Moreover, the need for accurate inverse kinematics becomes more challenging in such systems, where friction and compliance interact in complex ways.

The main aim of this project is to design and build a flexible, soft surgical robot actuated by cables, specifically targeting the challenges associated with friction and inverse kinematics. Careful consideration will be given to addressing friction related issues, ensuring smooth and accurate actuation. The development will involve detailed mathematical modelling of the cable-driven soft robotic system, incorporating the frictional dynamics and mechanical characteristics that come with soft actuators. Computer simulations were used extensively to simulate the robot's behaviour, enabling the validation and testing of inverse kinematics algorithms. These simulations serve as a critical bridge between theory and practice, informing design decisions and control strategies. The refined control algorithms developed in the simulations were then

implemented in a physical prototype to assess real-world performance, enabling closed loop control and verification of the system's accuracy and manoeuvrability in real world positions.

## **2 Background**

### **2.1 Overview of Robotic-Assisted Surgery**

Since the first case of using robots in surgery, in 1985 by Kwoh et al, to perform neurosurgical biopsies with greater precision, robotic assisted surgery has developed at a rapid pace (Lanfranco et al., 2004). At its core, robotic-assisted surgery integrates advanced mechanical systems, sensor technologies, and computational control to build upon and even enhance the surgeon’s capabilities, enabling complex procedures to be performed through small incisions with heightened dexterity and control.

Among the most extensively utilised and clinically validated platforms is the da Vinci Surgical System, developed by Intuitive Surgical. This system utilises the master–slave configuration, wherein the surgeon manipulates robotic instruments from a remote console, translating hand movements into finely tuned actions at the instrument tips. Equipped with articulating end-effectors with tremor filtration and high-definition stereoscopic vision, da Vinci has been widely adopted in urological, thoracic and cardiovascular surgeries, where precision in confined anatomical regions is critical (Intuitive Surgical, 2025).

Despite its demonstrable success, current robotic surgical platforms are constrained by fundamental limitations stemming from their rigid-link natures. These systems, while mechanically robust, lack the intrinsic compliance required to safely conform to the delicate and deformable structures of the human body. Their kinematic design is inherently ill-suited for navigating anatomical pathways, limiting their effectiveness in highly dynamic intraoperative environments. Furthermore, the reliance on rigid mechanics imposes constraints on instrument miniaturisation and forceful contact with tissue which are critical for advancing the frontiers of minimally invasive surgery.

These limitations underscore a need for surgical robotics that can overcome these issues. Emerging research is increasingly focusing on soft and flexible robotic architectures that can inherently adapt to the complexities of human anatomy. In particular, the integration of compliant materials, continuum structures, and cable or even pneumatic driven mechanisms offer a promising pathway toward safer, more versatile, and anatomically

friendlier surgical systems.

## 2.2 Soft Robotics in Surgical Applications

Soft robotics, unlike traditional rigid robots, focus on building robots from flexible and stretchable materials such as silicon and elastomers. This allows them to bend, twist and adapt their shape to more effectively navigate around the body's complex and changing anatomy. During surgery this natural flexibility allows them to interact more safely with soft tissue, reducing the risk of unintentional harm to the patient.

This reduced risk comes from the robot's ability to adapt completely passively to the surrounds. The soft materials they are made from, can conform to different shapes and absorb pressures that are applied to the robot, all without the need for very complex control systems and sensors. Zhang et al. (2015) for example, developed a robot that has a 2-part design, driven by 4 cables, which offers enhanced dexterity compared to traditional rigid robots, enabling it to navigate through complex and narrow spaces within the body by making unique shapes such as those seen below in Figure 1. This increased flexibility makes the robot well-suited particularly for applications in surgical scenarios where the environment is unpredictable, and tissues are often very fragile.

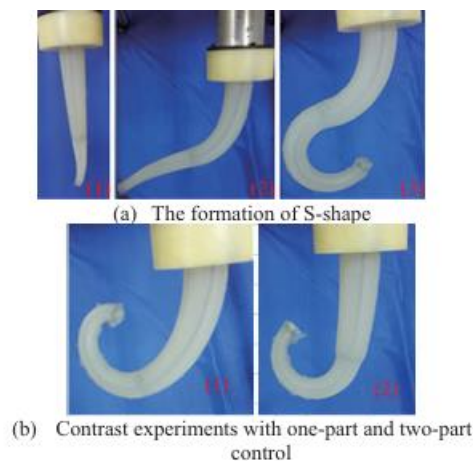


*Figure 1 - Motion analysis in non-restriction environment*

The choice of materials is central to the performance, safety, and reliability of soft robotic systems in surgical settings. These robots must be made from substances that are not only highly flexible and elastic, but also biocompatible, sterilisable, and mechanically durable under repeated use. The materials must allow for smooth movement and precise control



while also being safe to use inside the human body. Silicone-based elastomers are among the most used materials in soft surgical robots. These include commercially available formulations such as Ecoflex, Bentley Advanced Materials (2025), which possesses key characteristics such as excellent stretchability, softness, and its skin safe certification. These silicones can be moulded into complex shapes and maintain their mechanical properties over a wide range of movements. Their ability to recover after large deformations makes them ideal for soft robotics applications in surgical scenarios.

Other types of materials, such as thermoplastic polyurethanes (TPUs) in 3D printing, as looked at by Farid et al. (2024), and hydrogels, are also being explored. TPUs offer good strength and abrasion resistance, while remaining flexible. Hydrogels, which can hold large amounts of water and mimic the softness of biological tissues, show promise for highly sensitive applications, especially where gentle interaction with organs or vessels is required.

In more advanced applications, smart materials are being incorporated to introduce new functionalities. Enyan et al. (2024) looked into smart materials, which could respond to external stimuli such as heat, that return to a pre-defined shape. These materials offer the possibility of creating actuators that are compact, silent, and highly responsive which are important features in confined surgical environments.

Importantly, all materials used in soft robotic surgery must meet strict biocompatibility standards. They must not trigger inflammation or rejection responses when in contact with human tissues. In addition, they must withstand sterilisation methods such as autoclaving or chemical disinfection without degrading or changing their properties. These constraints significantly narrow the range of suitable materials and require careful testing during development.

### **2.3 Cable-Driven Actuation Systems**

Cable-driven actuation systems are a widely used method for transmitting motion and force in both traditional and soft robotic surgical tools. These systems use flexible cables, often made of steel or high-strength polymer fibres, to pull and steer robotic components from a distance. Because the actuation source, typically consisting of motors or servos,

can be placed outside the patient's body, such as in, Figure 2 below, done by Cheng, Wang and Desai (2017) where they designed and analysed a remotely actuated neurosurgical robot where cable-driven systems are especially useful for minimally invasive procedures where space is limited and precision is essential such as in neurosurgery.



*Figure 2 - The complete cable-driven remotely actuated neurosurgical robotic system, MINIR-II*

One of the key advantages of cable-driven mechanisms is their high flexibility and compactness. Cables can be routed through narrow and curved channels, enabling the design of slender instruments that can navigate deep within the body through small incisions or natural orifices. These systems also offer excellent force transmission and control resolution, making them well-suited for tasks requiring fine manipulation, such as endoscopic suturing or microsurgery.

In soft surgical robots, cable actuation is commonly used in continuum arms, steerable catheters, and soft robotic manipulators. The mechanical simplicity of cable systems allows for a wide range of motion with relatively few components, which is important for maintaining sterility and reducing mechanical failure risks. Moreover, by adjusting cable tension, it is possible to control the curvature and stiffness of soft robotic elements, further increasing their versatility during surgery.

Wang et al. (2019) detail the development and validation of an external force self-sensing technique for a 4-DoF (4 degrees of freedom) surgical robot end-effector as seen in Figure 3 and Figure 4 below. This method utilises a cable-tension disturbance observer and eliminates the need for dedicated force sensors, simplifying the system design and

potentially reducing costs.

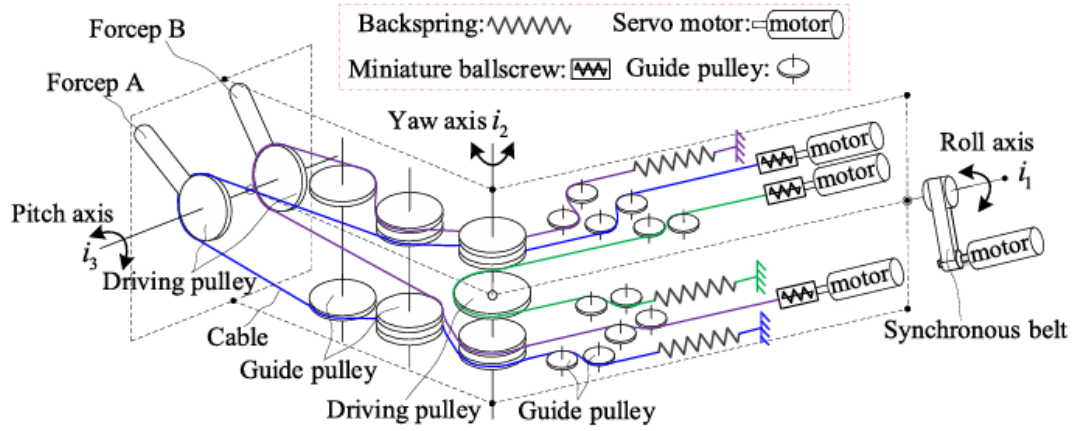


Figure 3 - Principle diagram of the 4-DoF surgical robot end-effector

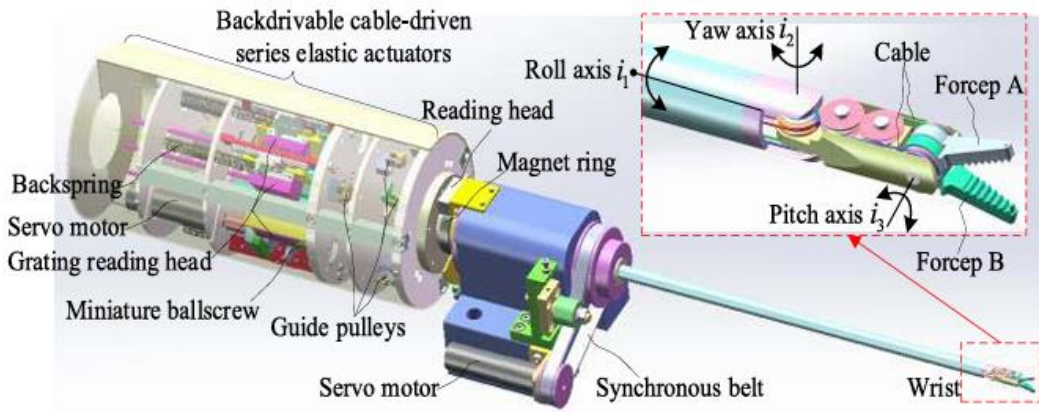


Figure 4 - 3D model of the 4-DoF surgical robot end-effector.

However, technical challenges remain, particularly when cables are used in soft or highly articulated systems. One of the primary concerns is friction, which occurs as the cable moves through guiding sheaths, bends, or around pulleys. This friction can lead to energy losses, delayed response, and reduced accuracy in positioning, especially over longer distances. Additionally, cable stretch and backlash, which is where there is a slight delay between input movement and actual response, can affect the precision and reliability of robotic motions.

Control systems must therefore compensate for these mechanical effects, often requiring complex modelling and calibration. Ensuring consistent performance over time is also

difficult, as cables may stretch or wear out with repeated use. These issues are particularly critical in surgical environments, where even small errors can have significant consequences.

## **2.4 Friction in Cable Actuated Robots**

In cable actuated robotic systems, friction arises primarily from the interaction between the cable and its surrounding environment, including guiding sheaths, pulleys, and the inner surfaces of flexible conduits. These interactions introduce resistance to motion that can lead to inaccuracies in control and degradation in system responsiveness.

One of the main sources of friction is the contact between the cable and the sheath, especially when routed through complex or highly curved paths. As the cable bends and slides within the sheath, normal forces increase at the points of curvature, which in turn increases friction. This effect becomes more pronounced as the number of bends or the radius of curvature decreases, resulting in higher resistance to motion and loss of efficiency. Pulleys and routing components, although designed to reduce friction, can also contribute to energy loss if not properly aligned or lubricated.

Material selection plays a significant role in frictional behaviour. Differences in surface roughness, hardness, and coating materials can affect the coefficient of friction between the cable and the sheath. In surgical settings, where sterilisation and biocompatibility must also be considered, options for low-friction materials are often limited. As such, achieving a balance between mechanical performance and clinical safety remains a significant design challenge.

Friction not only affects energy transmission but also introduces nonlinearities that complicate control. For instance, stick-slip behaviour where the cable momentarily sticks before suddenly slipping, can cause jerky or unpredictable movements, particularly at low speeds. Additionally, frictional hysteresis may result in a mismatch between intended and actual motion, making precise positioning of the surgical instrument more difficult to achieve.

Several methods have been explored to mitigate these issues. Mechanical solutions include optimised cable routing to minimise curvature, use of low-friction liner materials,

and implementation of tensioning mechanisms to maintain consistent preload in the cables. On the control side, friction compensation algorithms are often employed to correct for the expected losses and delays. Cheng, Wang and Desai (2017) in their Remotely Actuated Cable-driven Neurosurgical Robot, used nitinol wires inside Bowden tubes to attempt to ensure consistent friction for more predictable control. Pairing this with a static friction model helps estimate the friction coefficient, crucial for accurate control and force transmission.

## **2.5 Inverse Kinematics in Surgical Robotics**

Inverse kinematics (IK) is a central problem in robotics, concerned with determining the necessary joint configurations required to place a robot's end-effector at a specific position and orientation in space. In surgical robotics, where precision, responsiveness, and safety are paramount, solving the IK problem accurately is essential for guiding instruments along planned trajectories, maintaining consistent tool-tissue interaction, and enabling intuitive control during complex procedures.

In conventional rigid-link surgical robots, inverse kinematics solutions are often derived analytically. These analytical or closed-form solutions exploit the robot's specific geometric structure to produce exact mathematical expressions that map end-effector poses to joint variables. These methods are highly efficient and reliable when applicable. However, when the kinematic chain becomes more complex, or when redundancy is introduced to enhance dexterity and reachability, analytical approaches become ever increasingly complex and computationally demanding.

To address these more complex systems, numerical methods are commonly employed. Dulęba and Opałka (2013) looked at both classical and novel approximation techniques including Jacobian Pseudo-Inverse, Modified Levenberg–Marquard and others. While versatile, these methods must sacrifice either computational power or accuracy to achieve their intended goal.

Another approach frames the IK problem as a constrained optimisation task. In this formulation, the algorithm seeks to minimise the difference between the desired and current end-effector position while also considering secondary criteria such as joint limits,

obstacle avoidance, and smoothness of motion. This strategy is particularly well suited to redundant manipulators, where multiple joint configurations can achieve the same end-effector pose. Although powerful, optimisation-based IK can be computationally intensive and may converge to local minima, limiting its robustness in dynamic surgical environments.

As the field of surgical robotics evolves towards soft and continuum systems, IK becomes considerably more complex. Unlike rigid robots, soft robotic structures deform continuously along their bodies, lacking discrete joints. As a result, their configuration space is theoretically infinite-dimensional, and traditional IK methods no longer apply directly. One of the most common modelling approaches in this domain is the piecewise constant curvature (PCC) model, which approximates a soft continuum robot as a series of arcs with uniform curvature. This simplification reduces the system to a manageable number of parameters, making IK tractable through adapted geometric or numerical methods. However, the PCC assumption does not always hold in practice, particularly under external loads or in systems influenced by internal friction and material nonlinearity. Wild et al. (2024) tackled this issue by proposing their Piecewise Dual Quaternion (PDQ) kinematics-based algorithm which represents the robot's shape as a series of curved segments with constant curvature, just as shown below in Figure 5

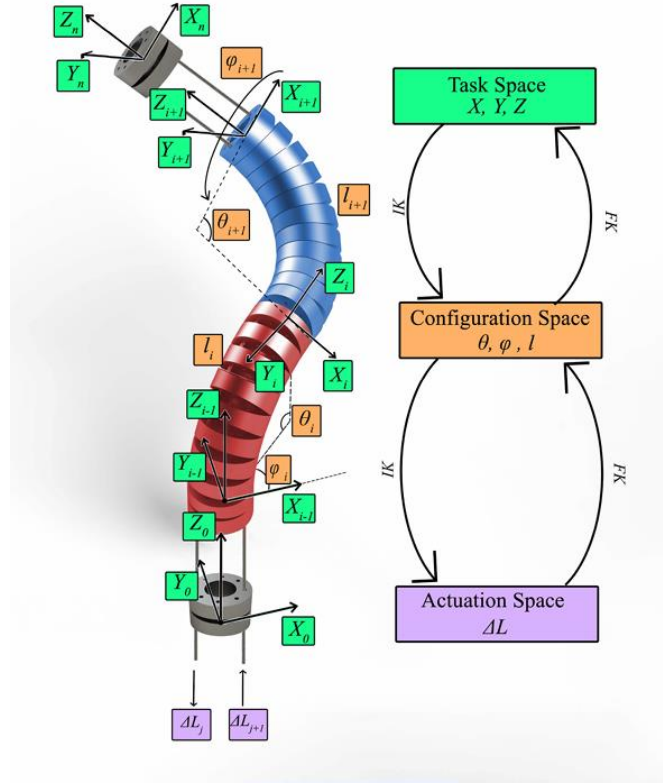


Figure 5 - Segmentation representation model for multi-section flexible robots

Other advanced strategies for soft robot IK include machine learning approaches such as the Kinematics-Informed Neural Network Yoon et al. (2024) worked on, which rely on training datasets generated through forward kinematics simulations or experimental data. Neural networks, can be trained to approximate the inverse mapping from end effector positions to control inputs. These methods are capable of modelling complex, nonlinear relationships that are difficult to capture with traditional models. Nevertheless, they require extensive training data and are sensitive to the quality and diversity of that data. They may also generalise poorly when confronted with scenarios that differ significantly from those seen during training.

Geometric and differential approaches, such as those based on spline curves or Frenet-Serret frames, have also been explored for modelling flexible backbones. These frameworks offer more physically intuitive representations and can be tuned to reflect real-world deformations, although they often require additional assumptions or boundary conditions to produce unique solutions. Keyvanara et al. (2023) addressed these challenges using a geometric optimisation-based IK model that discretises soft actuators

into rigid-link analogues, achieving high-precision trajectory tracking with secondary task prioritisation.

## **2.6 Control Strategies for Soft Robotic Systems**

The control of soft robotic systems, particularly those intended for surgical applications, presents a significant departure from the well-established techniques used in rigid robotics. Traditional control relies on precise models of kinematic chains and predictable joint behaviour; in contrast, soft robots exhibit nonlinear, time-varying, and often poorly defined dynamics due to their deformable structures and distributed actuation. This fundamental difference has driven the development of novel and hybrid control strategies aimed at ensuring accurate, stable, and safe performance in the demanding environment of the operating theatre.

One of the most widely used approaches in both rigid and soft robotic systems is proportional-integral-derivative (PID) control. Its simplicity, ease of implementation, and real-time responsiveness make it a useful starting point for controlling pressure, cable tension, or actuator displacement in soft robots. However, PID control alone often falls short when dealing with the unpredictable deformation, hysteresis, and coupling effects seen in soft structures. In response to these challenges, more advanced control methods have been introduced.

Model-based control strategies attempt to improve performance by incorporating a mathematical model of the robot's behaviour into the control law. For soft robots, this might involve geometric models such as the piecewise constant curvature approximation, dynamic models based on continuum mechanics, or empirical models derived from experimental data. Feedforward or inverse model control can then be used to pre-compensate for expected deformations. Cosimo Della Santina and Rus (2020) proposed a control-oriented polynomial curvature framework that captures higher-order deformation dynamics, enhancing robustness against nonlinear curvature changes. The accuracy of such approaches depends heavily on the fidelity of the model, which can be difficult to maintain in the presence of friction, variable loading, or material fatigue.

Adaptive control offers an alternative by allowing the controller to adjust its parameters



in real time based on observed performance. This method is particularly valuable for systems where the robot's physical properties change over time or vary between instances. In cable-driven soft robots, for instance, adaptive control can be used to compensate for cable slack or friction-related delays by continuously updating the controller based on sensor feedback. Wang et al. (2019) exemplified this approach by developing a self-sensing estimator using cable tension data to provide real-time feedback on joint motion and external force without dedicated sensors. The main limitation of adaptive approaches is the need for robust sensing and sufficient computational resources to maintain stability during adaptation.

Another increasingly popular technique is model predictive control (MPC), which uses an internal model to predict future states of the robot and select control actions that optimise performance over a short time horizon. MPC is well suited to soft robotics because it can handle complex constraints, nonlinearities, and time delays. However, the computational demands of MPC can limit its application in real-time systems, particularly when controlling high-degree-of-freedom structures or multiple actuators. Pal, He and Wei (2022)

Data-driven control methods, including neural network-based and reinforcement learning strategies, are also gaining ground. These controllers learn from data rather than relying solely on predefined models. This can be highly advantageous in soft systems, where exact modelling is difficult, and variability is high. For example, a neural network can be trained to approximate the relationship between actuator inputs and end-effector positions, effectively learning the system's inverse kinematics and dynamics. Reinforcement learning, though less mature in surgical contexts, has shown promise in developing control policies that optimise performance over time through trial and error. These methods, however, require large datasets, extensive training, and careful safety constraints all of which can be challenging in medical applications.

Hybrid control architectures are often employed to combine the strengths of different approaches. A soft surgical robot may use machine learning for inverse kinematics estimation and then combine that with closed-loop integral feedback control to enhance tracking accuracy (Arnau Garriga-Casanovas et al., 2024). As well as control

architectures, the integration of embedded sensing, such as fibre-optic shape sensors such as those studied by Xu (2017), enables feedback such as strain, torsion and curvature which can then be used to control the robot’s actual configuration, rather than relying solely on input-output estimation.

## **2.7 Gap in Current Research**

Despite significant advances in soft robotics and their increasing relevance to surgical applications, several critical gaps remain in the current body of research. These limitations span design, modelling, actuation, sensing, and control. These collectively hinder the transition of soft robotic systems from the laboratory to the operating theatre.

One of the most pressing challenges lies in the lack of reliable, real-time models that can accurately describe the behaviour of soft and cable-driven robots under surgical conditions. Existing kinematic and dynamic models often rely on simplifying assumptions as seen in piecewise constant curvature or uniform material properties. This doesn’t fully capture the complex interactions between soft bodies, actuation systems, and biological tissues, relying mostly on approximations. This modelling gap becomes even more problematic when friction, slack, and hysteresis are introduced through cable-driven mechanisms. Without high-fidelity models, control algorithms remain limited in their accuracy, adaptability, and robustness.

Closely related is the challenge of sensing and feedback in soft robotic systems. Unlike rigid robots, soft robots lack discrete joints from which to derive position or force data. While progress has been made in developing flexible and stretchable sensors, there is still no standardised, fully integrated sensing solution that offers high-resolution, multi-dimensional feedback without compromising the robot’s mechanical compliance or sterility. Many soft robots operate in open-loop or semi-closed-loop modes which as seen by Song et al. (2023), can reduce safety and precision in critical surgical contexts.

Control strategies for soft robots, particularly in real-time, high-stakes environments like surgery, remain in their infancy. While techniques such as model predictive control and adaptive learning have shown theoretical promise, their implementation is often hampered by high computational demands, reliance on idealised models, or the need for

large training datasets. There is a lack of clinically validated control systems that can reliably operate under dynamic intraoperative conditions, especially when unexpected interactions with tissue occur or when patient-specific variations arise.

The integration of actuation, sensing, and control into a single, cohesive platform presents another major hurdle. Many current prototypes are limited to proof-of-concept demonstrations that lack the robustness, modularity, and miniaturisation necessary for deployment in real-world surgical procedures. The absence of scalable fabrication methods and sterilisation-compatible designs further restricts their use in clinical trials and routine operations.

This project seeks to address some of these challenges directly, particularly those relating to modelling, control precision, and friction compensation in cable-driven soft robots by integrating IK formulations, control frameworks, and validated experimental prototypes.

## **3 Methodology**

### **3.1 Aims and Objectives**

The aims and objectives initially set out at the beginning of the project were as follows:

To design, simulate, and experimentally validate a cable-driven soft robotic manipulator with six DoF. This would be achieved by:

1. Conducting background studies on existing soft robotic surgical systems, inverse kinematics, and cable-driven actuation techniques.
2. To develop an initial 3-DoF physical prototype as a proof of concept.
3. Develop and understand the mathematics behind the inverse kinematics, friction and torque on the model
4. To create a MATLAB simulation environment by applying the mathematics from step 3
5. To design and fabricate a mould suitable for producing soft robotic segments using elastomeric materials.
6. Manufacture a 6-DoF soft robotic prototype and compare physical performance with simulated results.
7. To assess the controllability, accuracy, and fidelity of the final prototype through experimental analysis and simulation validation.

### 3.2 Initial Design

To validate the design of the soft robot, a concept design was made. The design was based on a SolidWorks model as seen in Figure 6. This model would consist of a repeating structure of solid backbones, either a plastic or metal for rigidity. The gaps between these rigid backbones would then be filled in with a soft, flexible material which would allow

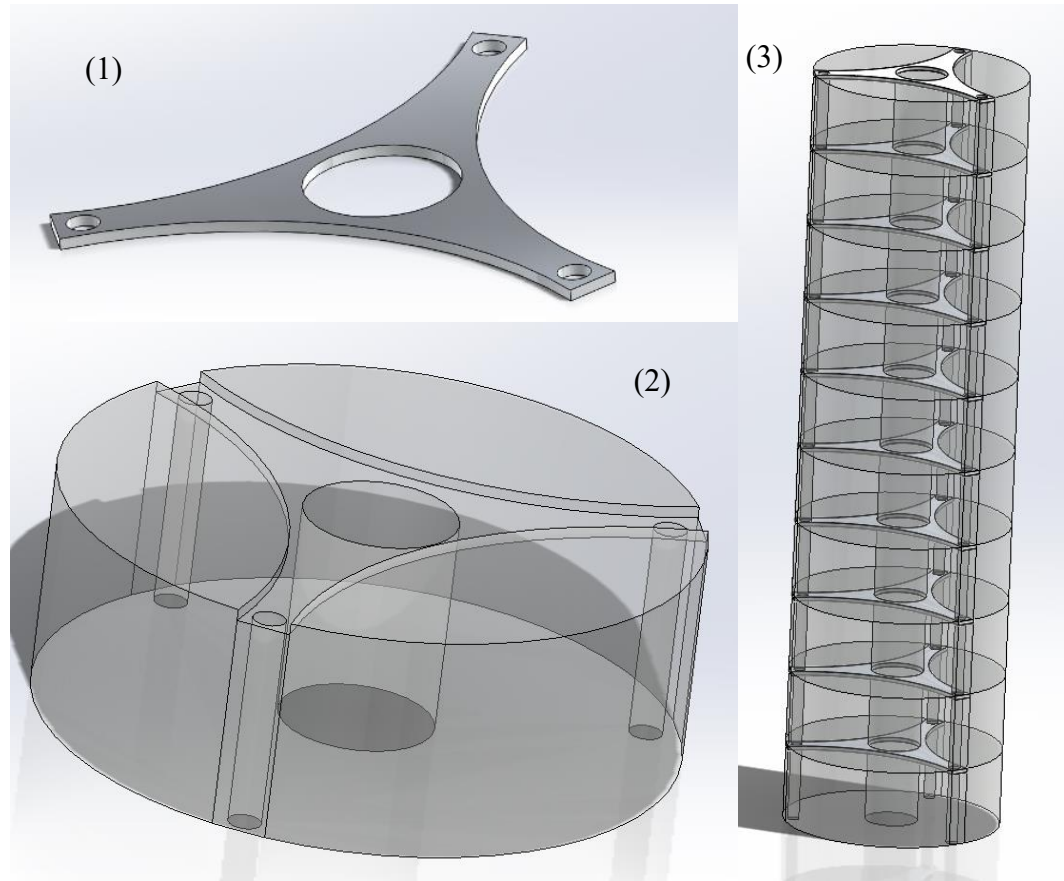
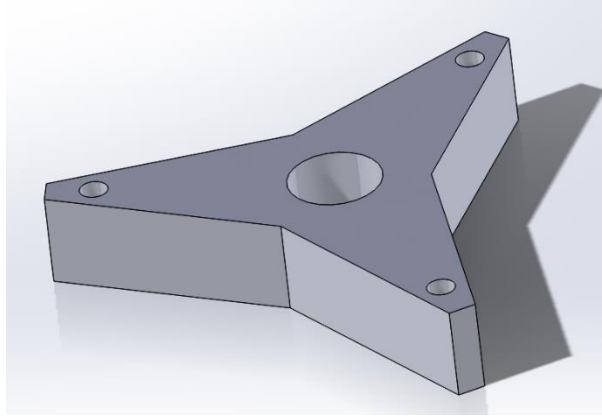


Figure 6 - (1) Rigid Spine (2) Soft, flexible material (3) Full Concept Design

the model to bend and flex. There are many types of soft filler material which could be used, as discussed by Li et al. (2019) ranging from elastomers all the way to special foams, each with their own distinctive advantages and disadvantages. In this case a synthetic material called Ecoflex 00-10 silicone would be selected for its easy use, versatility and skin safe certification after curing. This would come with difficult manufacturing challenges including the thin size of the rigid backbone sections and implementing them seamlessly with the silicone soft body structure.

### 3.3 3-DOF Spring-Based Model (Proof of Concept)

To overcome this problem initially and develop a proof-of-concept model, the model was scaled up to allow easy 3D printed on a standard fused deposition modelling printer (FDM). These rigid backbones can be seen in Figure 7. These models are made using polylactic acid (PLA) filament due to its high availability, cheap cost and its ability to be printed very easily.



*Figure 7 - 3D printable proof of concept backbone*

To replicate the flexing, a large spring was used to which multiple, in this case 5, of these backbones would be hot glued onto, allowing for the flexible movement of the model to

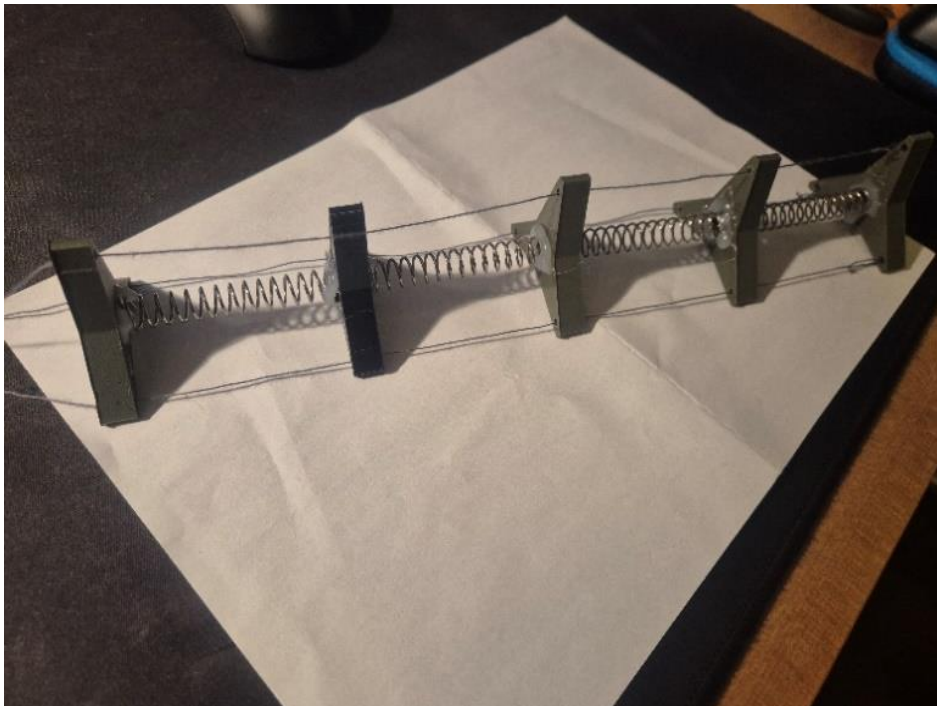


*Figure 8 - Proof of Concept model*

be retained. The spring has dimensions of 1x10x305mm, with each 3D printed backbone spaced evenly and equally apart. To actuate this, string was used. The final proof of concept model can be seen in Figure 8.

After that a platform was designed in SolidWorks to evaluate the functionality of the proof of concept.. This can be seen below in Figure 9 which shows the final proof of concept model in SolidWorks.



*Figure 9 - Proof of Concept Testing Setup*

This was then used to validate the design using an Arduino Nano to control the servo motors by manually inputting individual servo values to actuate the model.

### 3.4 Calculations

This section outlines the method for constructing arcs in three-dimensional space for modelling soft robotic limbs. The approach is geometric and parametric, allowing precise definition of curvature, plane orientation, and endpoints.

#### 3.4.1 Geometric Construction of an Arc

##### 3.4.1.1 Chord Length and Arc Length Relations

Arc 1 goes from  $P_1$  (origin) =  $(x, y, z)$  to  $P_2$  (first arc end / second start) =  $(x, y, z)_1$ , with  $L_1$  = length of Arc 1. Arc 2 starts at  $P_2$  and ends at  $P_3 = (x, y, z)_3$ , with  $L_2$  = length of Arc 2.

To construct an arc, we first calculate the chord length between two points  $P_A = (x_A, y_A, z_A)$  and  $P_B = (x_B, y_B, z_B)$  using the formula:

$$d = \sqrt{(x_B - x_A)^2 + (y_B - y_A)^2 + (z_B - z_A)^2} \quad (2)$$

This is valid only when  $L > d$ .

We relate the arc length to the chord length and radius by:

$$L = R\theta, \quad d = 2R\sin\left(\frac{\theta}{2}\right) \quad (2)$$

Substituting for  $\theta$  gives:

$$d = 2R\sin\left(\frac{L}{2R}\right) \quad (3)$$

##### 3.4.1.2 Midpoint and Arc Centre

The midpoint of the chord is:

$$M = \left(\frac{x_A + x_B}{2}, \frac{y_A + y_B}{2}, \frac{z_A + z_B}{2}\right) \quad (4)$$

From this, we calculate the height from the midpoint to the arc's centre:



$$h = \sqrt{R^2 - \left(\frac{d}{2}\right)^2} \quad (5)$$

#### 3.4.1.3 Plane Construction and Arc Orientation

We then construct the arc's plane. Starting with  $\vec{u} = (0,0,1)$ , we normalise the chord vector to get the unit vector  $\hat{v}$ . If  $\hat{v}$  is vertical, we instead use  $\vec{u} = (0,1,0)$ . The perpendicular component of  $\vec{u}$  to  $\hat{v}$  is:

$$\vec{u}_{\text{perp}} = \vec{u} - (\vec{u} \cdot \hat{v})\hat{v} \quad (6)$$

Normalising this gives the bending direction:

$$\vec{n} = \frac{\vec{u}_{\text{perp}}}{|\vec{u}_{\text{perp}}|} \quad (7)$$

#### 3.4.1.4 Applying Spin and Determining Arc Centre

To account for the arc's spin, we apply Rodrigues' rotation to  $\vec{n}$  about  $\hat{v}$  using angle  $\phi$ :

$$\vec{n}_{\text{rot}} = \vec{n}\cos\phi + (\hat{v} \times \vec{n})\sin\phi + \hat{v}(\hat{v} \cdot \vec{n})(1 - \cos\phi) \quad (8)$$

The centre of the arc is then:

$$C = M + h \cdot \vec{n}_{\text{rot}} \quad (9)$$

#### 3.4.1.5 Arc Parameterisation in 3D Space

To draw the arc in 3D, we define direction vectors:

$$\vec{e}_1 = \frac{P_A - C}{|P_A - C|} \quad (10)$$

$$\vec{e}_2 = \frac{P_B - C - R\cos\theta \cdot \vec{e}_1}{R\sin\theta} \quad (11)$$

The parametric equation for the arc is:

$$P(t) = C + R\cos t \cdot \vec{e}_1 + R\sin t \cdot \vec{e}_2, \quad t \in [0, \theta] \quad (12)$$

We ensure that the arc remains within the positive z plane by numerically testing

different spin angles.

### 3.4.2 Torque Due to Cable Offset

We now analyse the torque applied at the base of a soft robot due to a cable offset and curvature. Let  $L$  be the arc length,  $R$  the radius, and  $\theta = \frac{L}{R}$ . Assuming deformation in the  $x$ - $z$  plane, a point on the arc is defined by:

$$x = R\sin\theta \quad (13)$$

$$z = R(1 - \cos\theta) \quad (14)$$

Thus, the tip position is:

$$\vec{r}_{\text{tip}} = (R\sin\theta, 0, R(1 - \cos\theta)) \quad (15)$$

If the cable is offset horizontally by  $r_{\text{offset}}$ , the cable position becomes:

$$\vec{r}_{\text{cable}} = (R\sin\theta + r_{\text{offset}}\cos\theta, 0, R(1 - \cos\theta) + r_{\text{offset}}\sin\theta) \quad (16)$$

A vertical downward force is applied:

$$\vec{F} = (0, 0, -F) \quad (17)$$

The resulting torque is given by:

$$\vec{M} = \vec{r}_{\text{cable}} \times \vec{F} = (0, F(R\sin\theta + r_{\text{offset}}\cos\theta), 0) \quad (18)$$

As only the horizontal component contributes to torque, we define the effective lever arm as:

$$d_{\text{eff}} = R\sin\theta + r_{\text{offset}}\cos\theta \quad (19)$$

The resulting moment magnitude is:

$$M = F \cdot d_{\text{eff}} = F(R\sin\theta + r_{\text{offset}}\cos\theta) \quad (20)$$

### 3.4.3 Frictional Effects in Cable-Driven Soft Robotics under Curvature

In cable-driven soft robotic systems, the routing of cables through curved and deformable channels introduces frictional forces that must be accounted for in both control and mechanical design. As the soft structure bends, the cables experience increased surface contact and normal force within the internal conduits, leading to a rise in friction that can affect actuation precision and responsiveness.

The frictional force experienced by a cable constrained within a curved path is commonly modelled using the *capstan equation*, a well-established relation in contact mechanics. This equation describes the exponential relationship between the input and output tensions of a flexible element wrapped around a surface with friction:

$$T_2 = T_1 e^{\mu\theta} \quad (21)$$

where:

- $T_1$  is the tension on the entry side of the curvature,
- $T_2$  is the tension on the exit side,
- $\mu$  is the coefficient of static friction between the cable and the conduit surface,
- $\theta$  is the total wrap angle in radians over which the cable is in contact with the curved surface,
- $e$  is Euler's number.

The difference in tension,  $F_{\text{friction}} = T_2 - T_1$ , represents the net frictional force introduced due to the curvature. This relation illustrates that even moderate increases in the wrap angle or the friction coefficient can lead to substantial exponential growth in frictional resistance, which is particularly relevant in soft robots with complex, multi-segmented geometries.

The wrap angle  $\theta$  can be related to the geometry of the robot's deformation by the following expression:

$$\theta = \frac{L}{R} \quad (22)$$

where:

- $L$  is the arc length of the cable in contact with the internal surface,
- $R$  is the local radius of curvature of the robot segment.

Substituting this into the capstan equation provides a means to quantitatively evaluate the impact of a given curvature on cable friction. In systems with multiple curvature points, such effects may accumulate, resulting in significant performance degradation unless actively accounted for through control algorithms or design optimisation.

It is also important to note that the capstan equation models *static* friction; dynamic friction may differ depending on the velocity of cable movement and material properties, and may require additional modelling in high-speed or continuously actuated systems.

### 3.5 MATLAB Simulation

#### 3.5.1 3 DoF Model

Building on the calculations outlined in the prior section, a simulation was developed in MATLAB to visualise the resulting arc geometry. This simulation enables the user to input a specific end point (marked with a grey star), upon which the model generates a curved path between the start and end positions. An interactive slider was integrated into the interface, allowing for dynamic rotation of the curve about the chord (dotted line) connecting the two points. A key design constraint was to ensure that the curve does not intersect or fall below the x-y plane, which represents the ground in the simulation environment.

At this stage of development, the simulation focuses solely on the geometric generation of a spatial arc and does not incorporate any cables. The model operates under idealised conditions, without accounting for external forces, material properties, gravity, or friction. It is intended as a purely kinematic representation to explore the feasibility of generating valid curved paths that comply with basic spatial constraints.

### 3.4.2 6 DoF Final Model

Following the development of the initial 3 DoF simulation, the next phase focused on extending the model to 6 DoF, with the additional objective of integrating physical actuation. This allowed a real-world soft robotic prototype to replicate the bending behaviour observed in the simulation. To achieve this, a MATLAB-based control environment was developed to interface the simulated kinematics with an Arduino-actuated soft robot.

The environment combines three-dimensional visualization, interactive parameter adjustment, real-time torque estimation, and direct serial communication with an Arduino Nano microcontroller. Six servo motors, each corresponding to one of the robot's tendons, are controlled through this setup, enabling the physical model to mirror its virtual counterpart.

The simulation begins by accepting two sets of user-defined three-dimensional coordinates that represent intermediate and terminal bending points of the robot. Using these as geometric constraints, the system computes two connected circular arcs to emulate the robot's curvature. Each arc is derived from a known arc length and its associated chord, ensuring that the specified configuration is physically achievable. A midpoint-based method is employed to construct the arc's plane, and Rodrigues' rotation formula is used to allow spin angle flexibility around the arc's chord. The simulation further evaluates a complete 360-degree range of spin angles to identify all valid configurations in which the resulting arc lies entirely within the non-negative z-domain, corresponding to upward bending within a practical workspace.

Each arc is associated with three actuation cables, positioned at a fixed radial offset from the arc's centerline. These cables, coloured orange for the first arc and light blue for the second, are routed along the arc, as can be seen in Figure 10, using a local coordinate frame composed of tangent, normal, and binormal vectors. At every discretized segment along the arc, the cables are offset according to this frame to maintain consistent orientation and spatial alignment. The total length of each cable is computed by integrating the segment-wise Euclidean distances along the cable path. To ensure continuity, the initial offset vectors for the second arc are determined based on the

terminal configuration of the cables from the first arc.

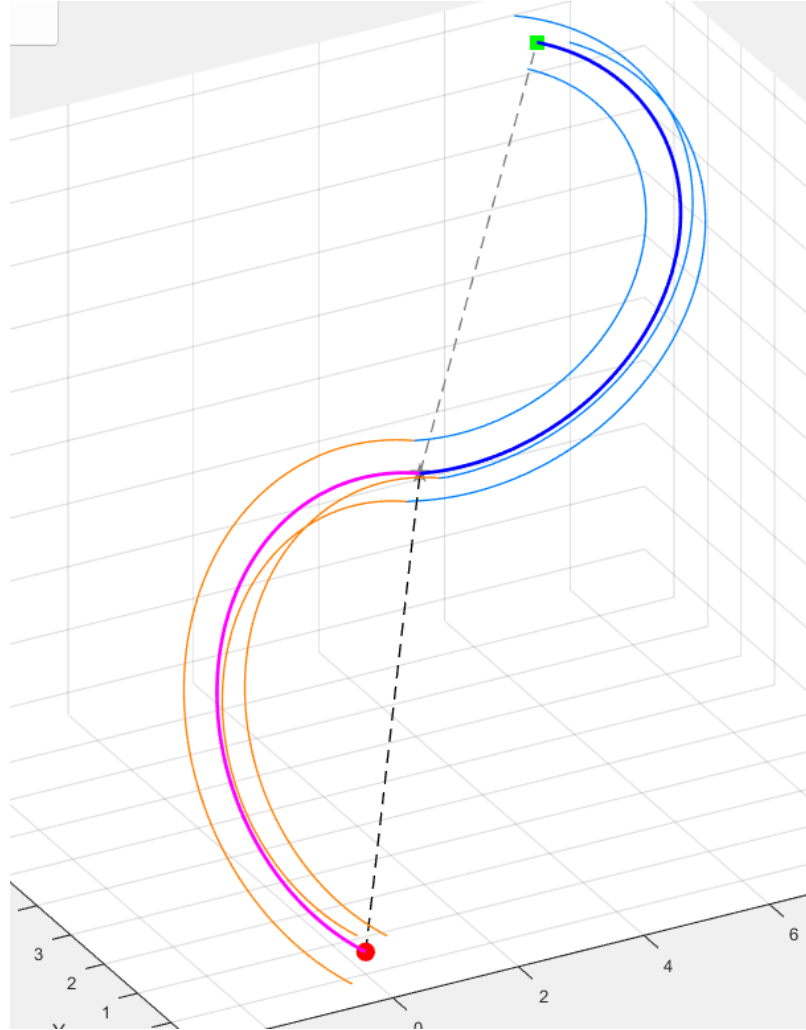


*Figure 10 - Cable Routing in MATLAB Simulation*

Communication with the Arduino Nano is managed via MATLAB's serial port interface. By comparing the current cable lengths to those from the previous state, the system determines the necessary adjustments for each tendon. The servos are driven by pulse-width modulation (PWM) signals, with a neutral angle of 90 degrees corresponding to no movement. Depending on whether the cable needs to be retracted or extended, the servo is temporarily set to either 60 degrees or 120 degrees. The actuation duration is linearly scaled according to the magnitude of the cable length change, with thresholds in place to suppress minor adjustments and prevent mechanical jitter or overextension. Each update cycle sends both angle and duration vectors to the Arduino, which executes the motion before returning the servos to their neutral positions. This strategy ensures consistent tendon positioning and avoids idle drift or cumulative error.

The physical implementation involves wiring the Arduino Nano directly to six servo motors via digital pins D2 through D7, as seen in Figure 11. Each pin is assigned to a dedicated servo channel, corresponding to one of the robot's tendons. The servos are controlled using standard PWM signals, with pulse widths typically ranging from 1 millisecond to 2 milliseconds, representing angles from 0 degrees to 180 degrees. An Arduino sketch was written to receive serial commands over USB, interpret the angle-duration format, and actuate each motor accordingly.

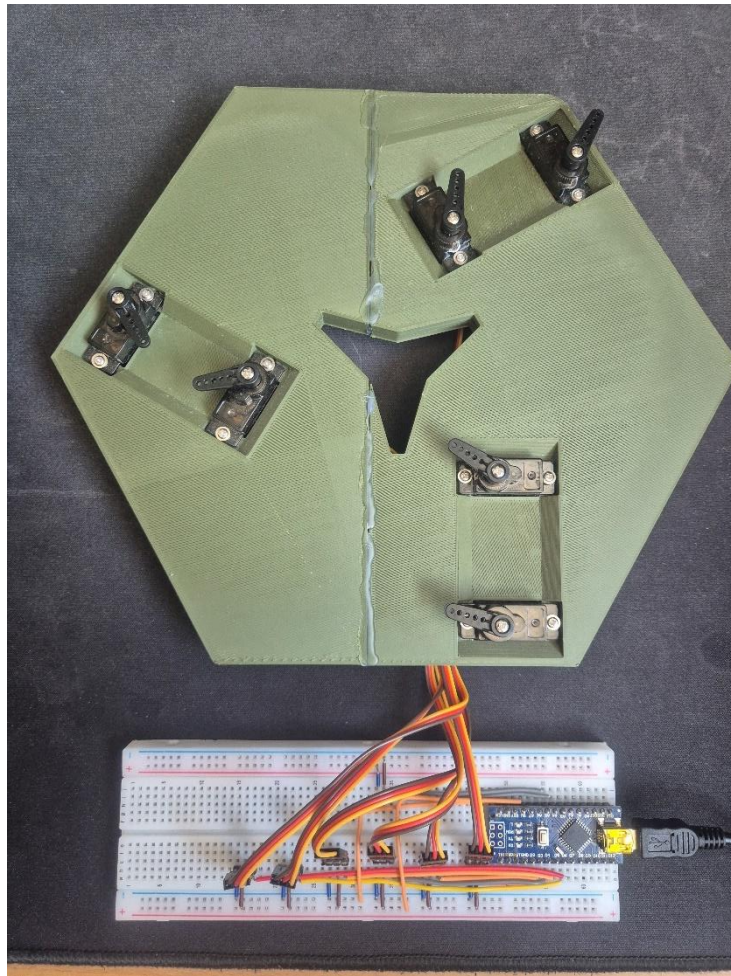


*Figure 11 - Electronic Control Setup*

The MATLAB interface includes graphical components for modifying endpoint coordinates, adjusting pulling force, and varying the spin angles of the arcs. It provides real-time feedback by updating the displayed arc geometries, cable paths, torque calculations, and cable lengths. All state information, including geometric parameters and the active serial connection, is stored in the application data of the MATLAB figure, allowing smooth data management and user interaction.

Upon closing the simulation, all resources such as open serial ports and user interface handles are properly released, ensuring safe disconnection from the Arduino and avoiding residual communication conflicts during subsequent operation.

### **3.6 Mould Design and Fabrication of 6 DoF Model**

Following the completion of the simulation phase, the next step involved designing and fabricating a mould for casting the final soft robotic prototype. The mould was initially developed using SolidWorks, where particular attention was given to dimensional tolerances to ensure that the individual components would fit together precisely and could be assembled and disassembled with ease. Considerable care was taken to simplify the design in order to facilitate removal of the cured Ecoflex material, which tends to adhere strongly to the mould surfaces.

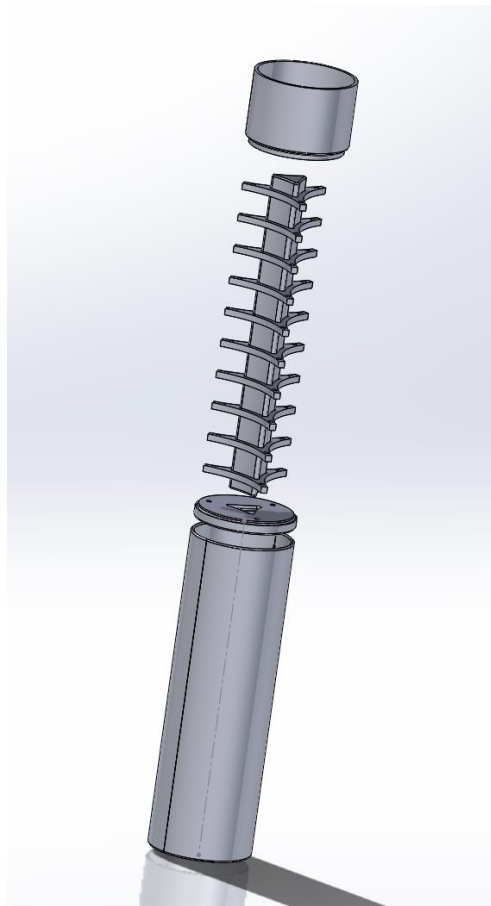


*Figure 12 - Mould Design*

To achieve the required precision and tight tolerances, the mould was fabricated using a high-resolution resin-based 3D printer. The resulting mould design is shown in Figure 12



above.

Given the thin and delicate nature of the intended cable channels, it was determined that 3D printing these features would not provide sufficient mechanical integrity. Instead, metal straight ejector pins were selected and integrated into the mould to form the cable channels during casting. These pins were chosen based on their exact diameter and appropriate length, which allowed for straightforward insertion and removal without damaging the cured silicone structure. The pins can be Part (1) of Figure 14 alongside the rest of the successfully 3D printed resin parts.

Once all components of the mould had been successfully printed, they were assembled in preparation for casting the Ecoflex mixture. To ensure the mould remained securely closed throughout the curing process, while still allowing for easy disassembly afterward, zip ties were used as a non-permanent fastening method as seen in Part (2) of Figure 13. This method provided sufficient clamping force to hold the mould components firmly together while avoiding the use of more complex fastening solutions that could complicate removal of the final silicone part. As well as that, any areas where the liquid mixture could leak out was sealed with regular sticky tape. This was done to make sure removal was as easy as possible as well as making sure that the mould could be re-used

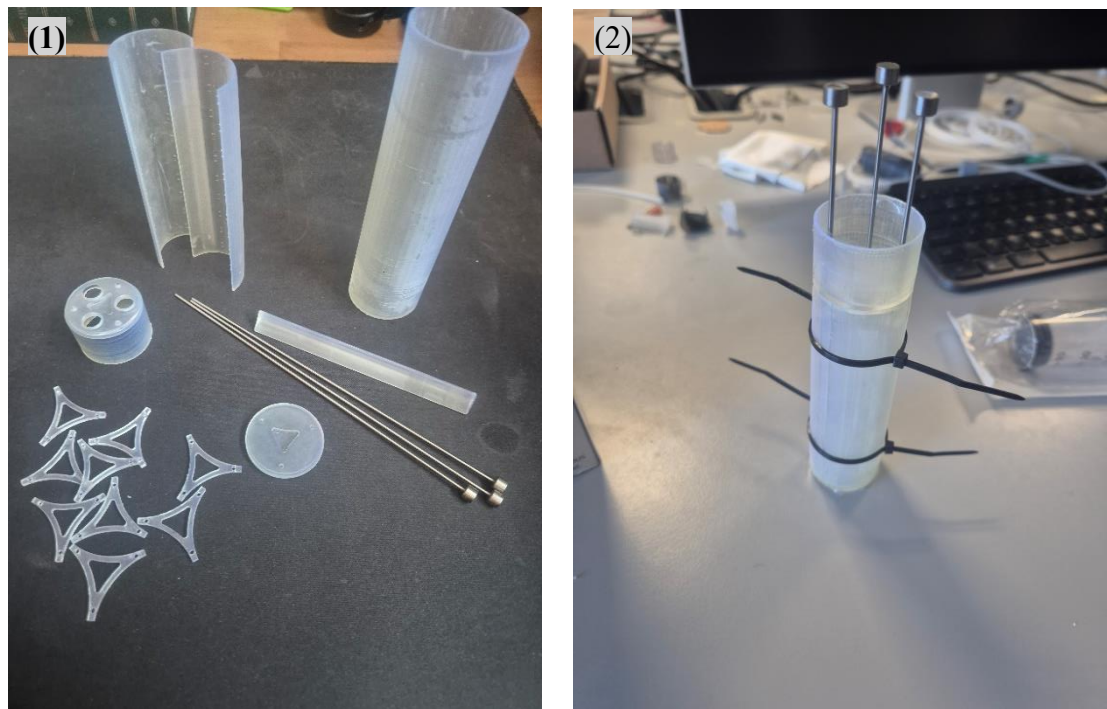


*Figure 13 - (1) Mould Components After Printing (2) Fully Assembled Mould*

again.

The next step was to prepare the Ecoflex mixture. Ecoflex 00-10 is made of two parts, as seen in Part (2) of Figure 14, that need to be mixed in a 1A:1B ratio of volume or weight as seen on the packaging material below in Part (1) of Figure 14.

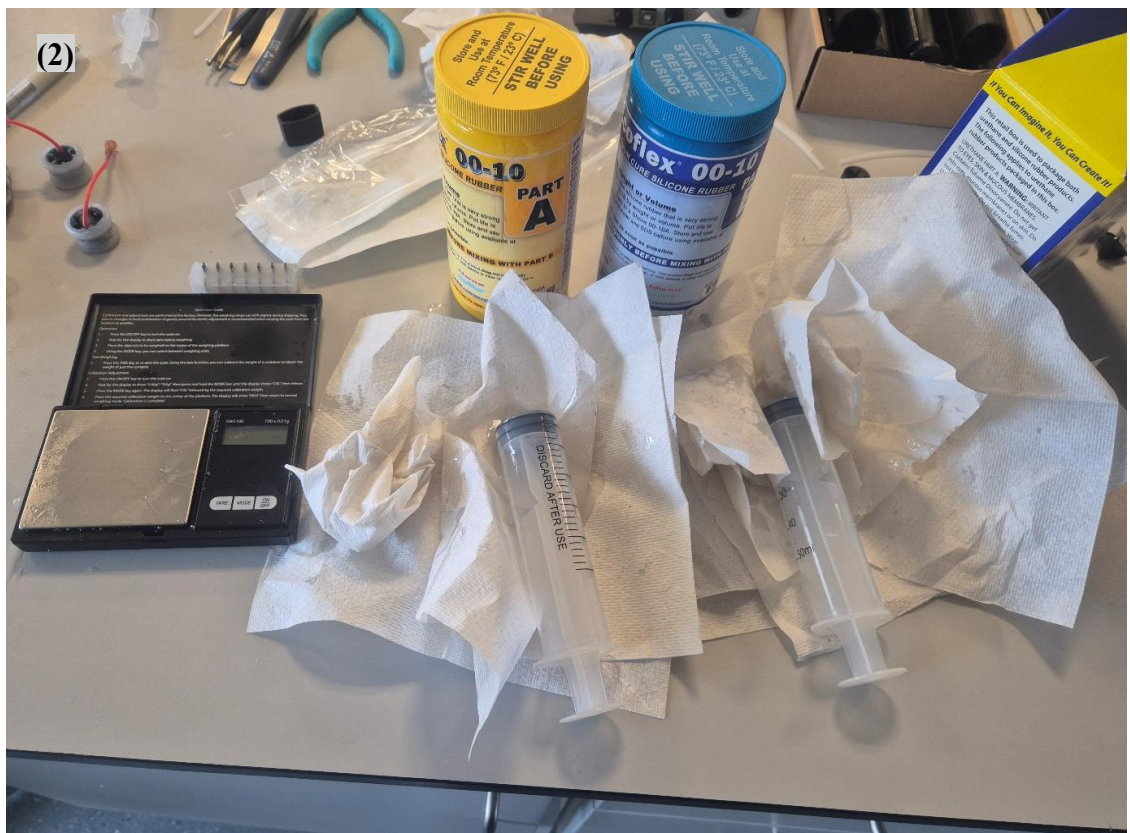


Figure 14 - (1) Ecoflex 00-10 Packaging (2) Mixing Process of Both Parts of Ecoflex Mixture

In a small container, 30 grams of each part was measured on a scale and combined and after thorough mixing, was placed into a vacuum oven for 20 minutes to get rid of any trapped air inside of the mixture as seen in Figure 15. It is important to remove as much



Figure 15 - Vacuum Oven Air Removal

air particles from the mixture as possible to avoid air bubbles being trapped in the final mould. This could cause catastrophic damage or unpredictable deformation once cured.

After that, the mixture was carefully transferred to the mould and then placed in an oven at 60° Celsius for 20 minutes as seen in Figure 16.

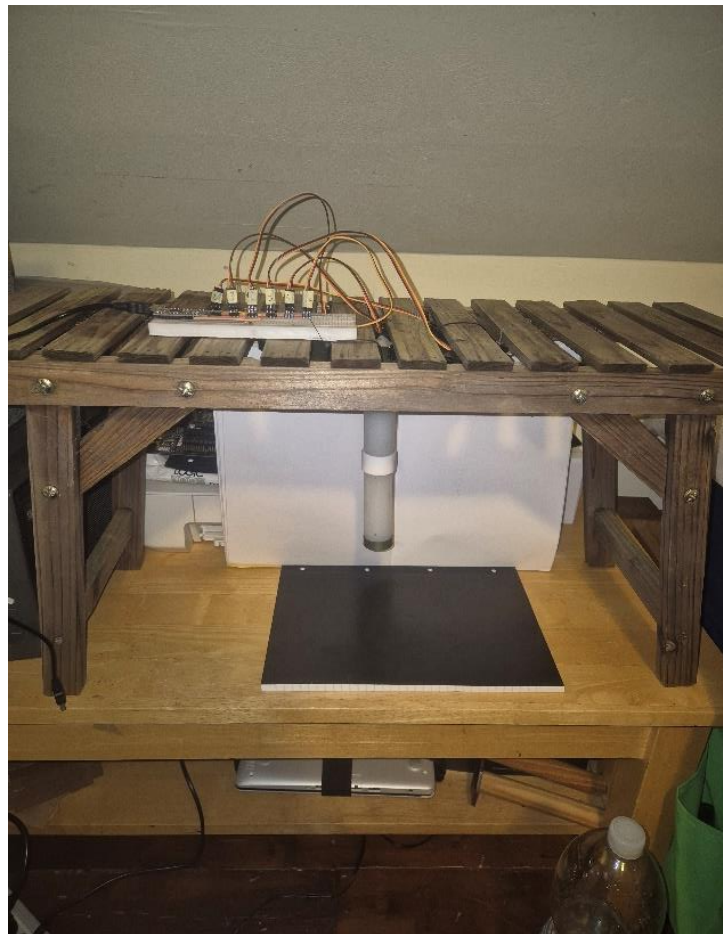


Figure 16 - Curing Inside Oven at 60° Celsius for 20 Minutes



After removing from the oven, the mixture was given another 3-4 hours to cure in room temperature before carefully removing the mould.

The mould was then put back together and the process repeated for a second time to obtain the second part of the 6 DoF prototype. As well as that, connector pieces were 3D printed to simplify the connection between each of the silicon parts as well as the base. To route the actuation cables, a needle and string were employed to guide the cables through the pre-formed channels in the silicone. Each cable was then secured in place using hot glue at the terminal ends of both the first and second segments. The opposite ends of the cables were similarly glued to the rotators attached to the servo motors. Finally,



*Figure 17 - 6 DoF Prototype Mounted on Test Bench*

the entire assembly was mounted in an inverted orientation, as shown in Figure 17, allowing the default home position of the robot to correspond with a vertically downward alignment. Wires were managed through the bench to avoid interfering with the model.

## 4 Results

### 4.1 Software Simulation

This section presents the outcomes of the MATLAB-based simulation and control interface. It includes both the 3-DoF arc simulation for geometric proof-of-concept and the full 6-DoF simulation integrated with servo control via an Arduino Nano. The interactive Graphical user interface (GUI) used for adjusting arc parameters, observing cable length variations, and visualising torque is also discussed.

#### 4.1.1 3-DOF Arc Simulation (Proof of Concept)

The 3-DoF simulation was developed to validate the geometric arc generation method using a single spatial arc. The algorithm accepted user-defined endpoint coordinates and successfully generated an arc within workspace constraints, ensuring no intersection with the negative z-domain. Additionally, a slider to allow the user to rotate the path of the curve around the chord making sure to still adhere to the previously addressed constraints.

Figure 18 below shows the MATLAB output of a 3-DoF arc, highlighting the arc path,

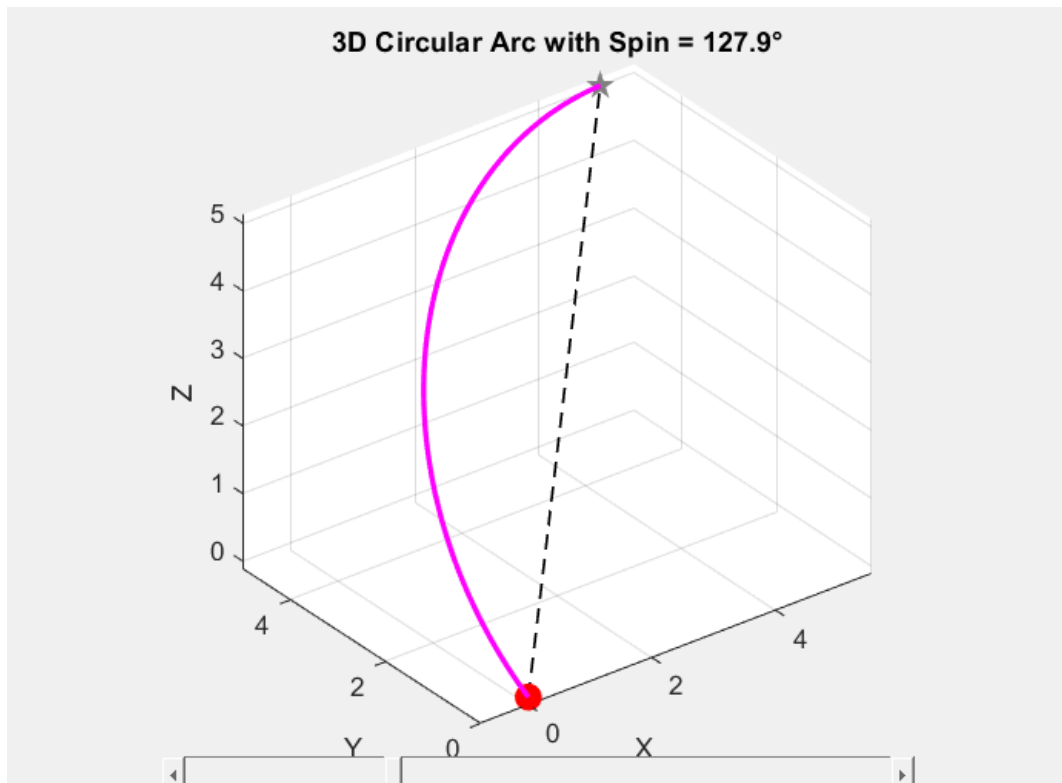


Figure 18 - 3 DoF Simulation Output

the start and end points, and the calculated chord.

### 4.1.2 6-DOF Arc Simulation and Cable Mapping

The full simulation extended the concept to two connected arcs, providing a 6-DOF representation. The GUI included input fields for endpoints, live force adjustment via sliders, and spin angle control for each arc. Cable lengths were dynamically calculated and displayed, with visualisation of tendon routing using radial offsets.

Figure 19 shows the 6-DoF simulation, complete with interactive sliders and cable length feedback. Torque estimation is displayed in real time based on user-set pulling force values.

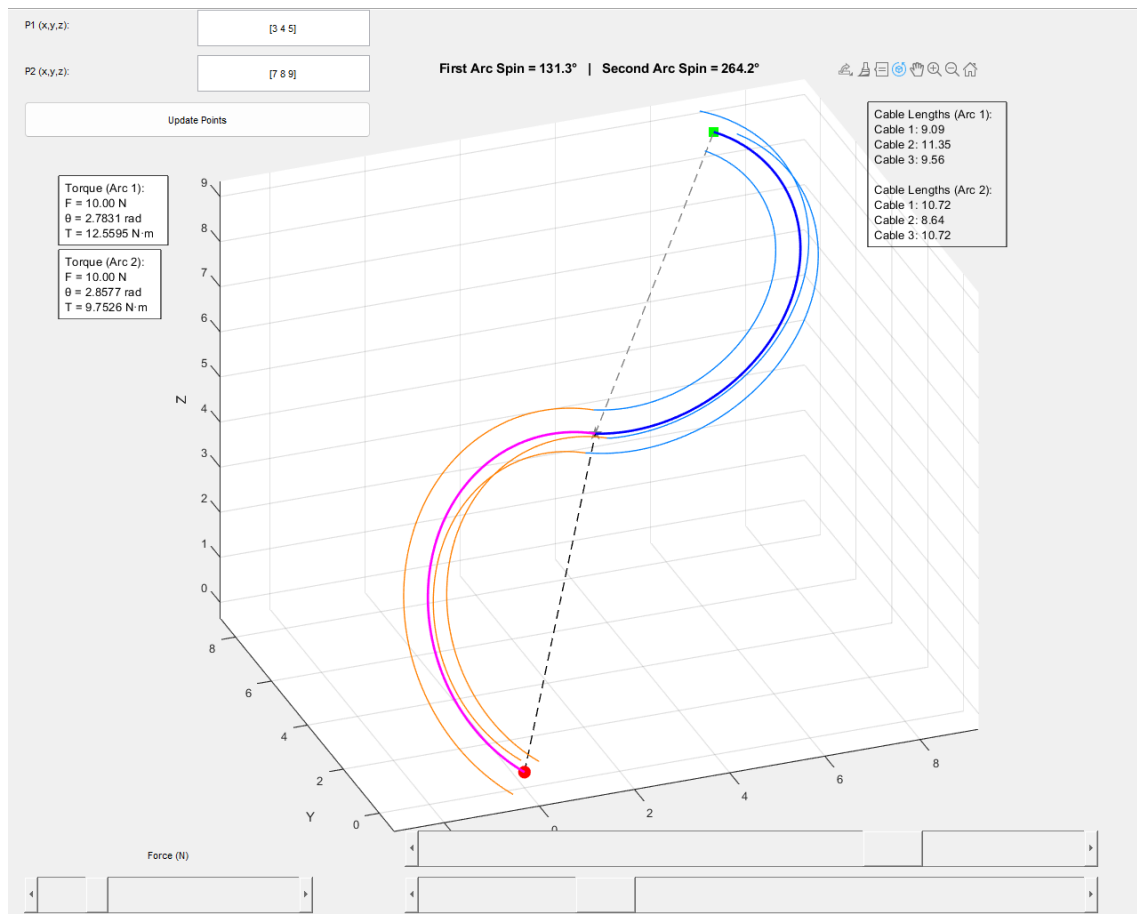


Figure 19 - 6 DoF MATLAB Simulation Output

Figure 20 shows an example position being translated into servo angles and duration instructions being logged and transmitted to the Arduino from the MATLAB command window. The timing values are not calibrated at this stage.

```
Sent servo angles and durations:
    60    120    120    120    60    60

    9.7037    1.3888    8.3149    8.6888    2.0849    7.5934

Stopped servo 2 at t = 1.39 s
Stopped servo 5 at t = 2.09 s
Stopped servo 6 at t = 7.59 s
Stopped servo 3 at t = 8.32 s
Stopped servo 4 at t = 8.70 s
Stopped servo 1 at t = 9.72 s
```

*Figure 20 - Example Position Servo Angles and Spin Duration Instructions*

## **4.2 Hardware Prototyping and Actuation**

The physical implementation consisted of a scaled 3-DoF printed model (proof of concept) and a full 6-DoF soft robotic manipulator fabricated using Ecoflex silicone and custom-designed moulds.

### **4.2.1 3-DOF Printed Model**

A flexible backbone prototype was constructed using PLA 3D printed segments mounted on a spring. The model was manually actuated using string attached to servo motors using direct inputs from the Arduino Nano for each individual servo.

Figure 21 illustrates the completed 3-DoF proof-of-concept model in both neutral and actuated positions.

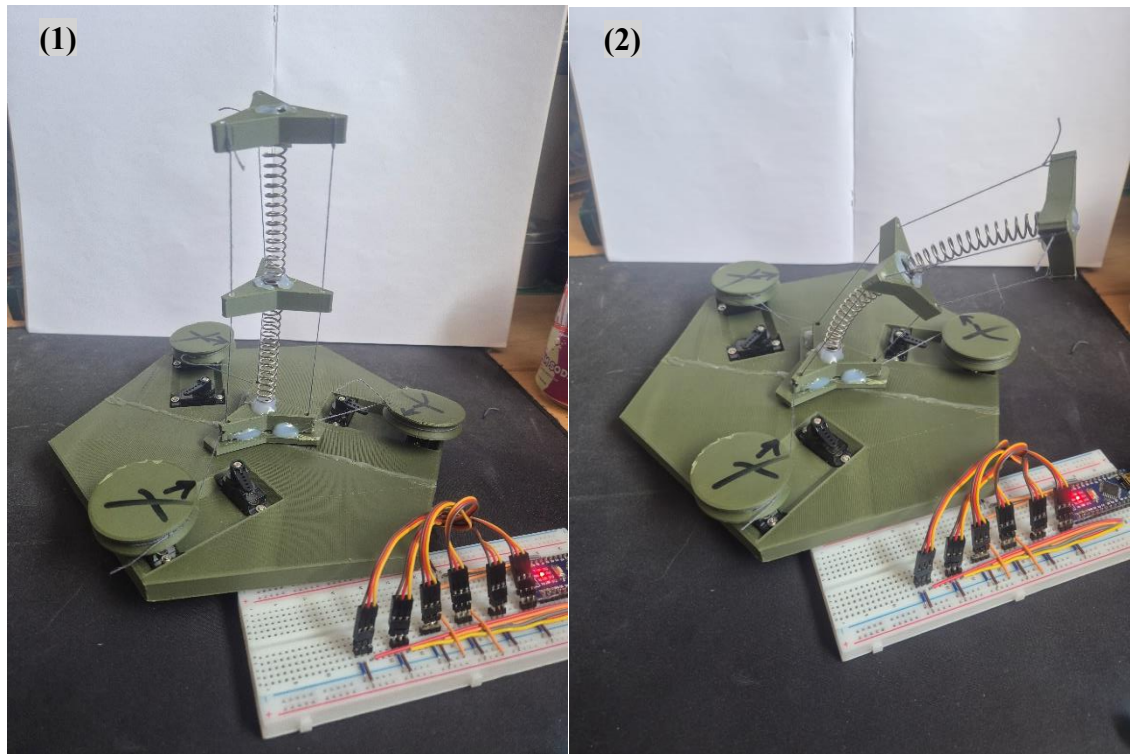


*Figure 21 - 3 DoF Proof of Concept in (1) Neutral Position (2) In Actuated Position*

#### **4.2.2 Final 6-DOF Soft Robotic Limb**

The full 6-DoF prototype was manufactured using two-part moulds designed in SolidWorks and printed in high-resolution resin. Cable channels were formed using embedded metal ejector pins. The Ecoflex 00-10 silicone was vacuum degassed, cast, and cured to produce compliant, biocompatible segments.

Figure 22 shows the mould components with embedded ejector pins just after vacuum and oven treatment.



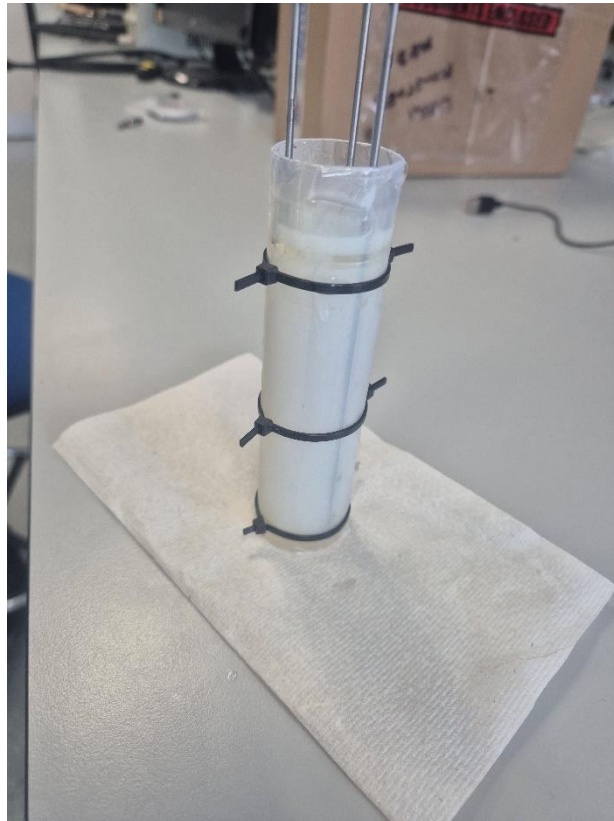


*Figure 23 - Mould after Vacuum and Oven Treatment*

Figure 23 shows the Ecoflex segments post-curing, alongside all of the required 3D printed connector pieces.



*Figure 22 - Disassembled Parts of 6 DoF Model*

Figure 24 displays the final assembled 6-DoF manipulator connected to the Arduino-controlled servos.



*Figure 24 - Final 6 DoF Model Assembly on Test Bench*

## **5 Discussion**

### **5.1 Performance of the Simulation Environment**

The simulation environment developed in MATLAB provided a comprehensive platform for validating the geometric and control principles of the soft robotic manipulator. The use of two connected arcs enabled the modelling of complex spatial bending with manageable computational demands. The system dynamically evaluated spin angles for each arc and excluded configurations that violated physical workspace constraints, such as arcs entering the negative z-domain. This ensured that all generated trajectories were feasible for physical implementation.

The GUI contributed significantly to the usability of the system. It allowed the user to modify parameters such as endpoint positions, spin angles, and cable force in real time while visualising the corresponding geometric and mechanical outputs.

Despite these advantages, the simulation environment operated under ideal assumptions. Real-world phenomena such as gravity-induced deformation, variable material stiffness, and external loading were not considered. As a result, while the simulation was effective for qualitative validation and initial control parameter tuning, it lacked the precision required to predict actual limb deformation under surgical or load-bearing conditions. To address these limitations, future simulation environments could incorporate more advanced mechanical models that include external forces, gravitational effects, and material nonlinearity. This could be achieved through finite element modelling or continuum mechanics-based approaches that would better capture the complexities of soft material deformation. This however would also come at a cost of higher computational power requirements.

## 5.2 Hardware Performance and Limitations

The initial 3-DoF spring-based prototype demonstrated relatively simple and predictable actuation behaviour. Its mechanical structure, built with rigid elements and linear elastic springs, allowed for straightforward cable-driven control. Although deformation did not always follow a smooth or idealised curvature, as can be seen in figure 25, where some sections bent more than others, the system in general, responded well to input.

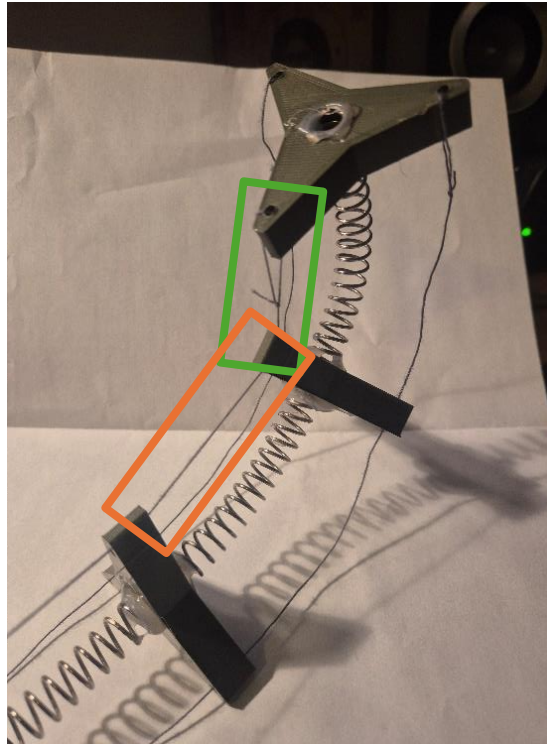


*Figure 25 - Display of Irregular Deformation in Proof of Concept*

Friction was present within the cable pathways, but it remained largely manageable at this scale due to the limited areas of contact between the cable and the rigid parts. This in turn did not impede the motion or the responsiveness of the prototype in a noticeable way.

In contrast, the 6-DoF Ecoflex-based prototype presented a marked shift in behaviour. The use of the Ecoflex silicone provided more natural and closer to the predicted simulated deformation. However, this increase in flexibility and DoF came with a considerable rise in actuation complexity. As the curvature increased across multiple segments, friction within the internal cable sheaths intensified significantly. This added resistance caused the servo motors to strain and, in several cases, fail to actuate the structure altogether. The maximum range of movement before major issues arose such as

actuation failure or snapping cables can be seen below in Part (1) of Figure 26 alongside the intended simulated result in part (2) of Figure 26. Note that the real robot image is flipped 180 degrees to show comparison more clearly.

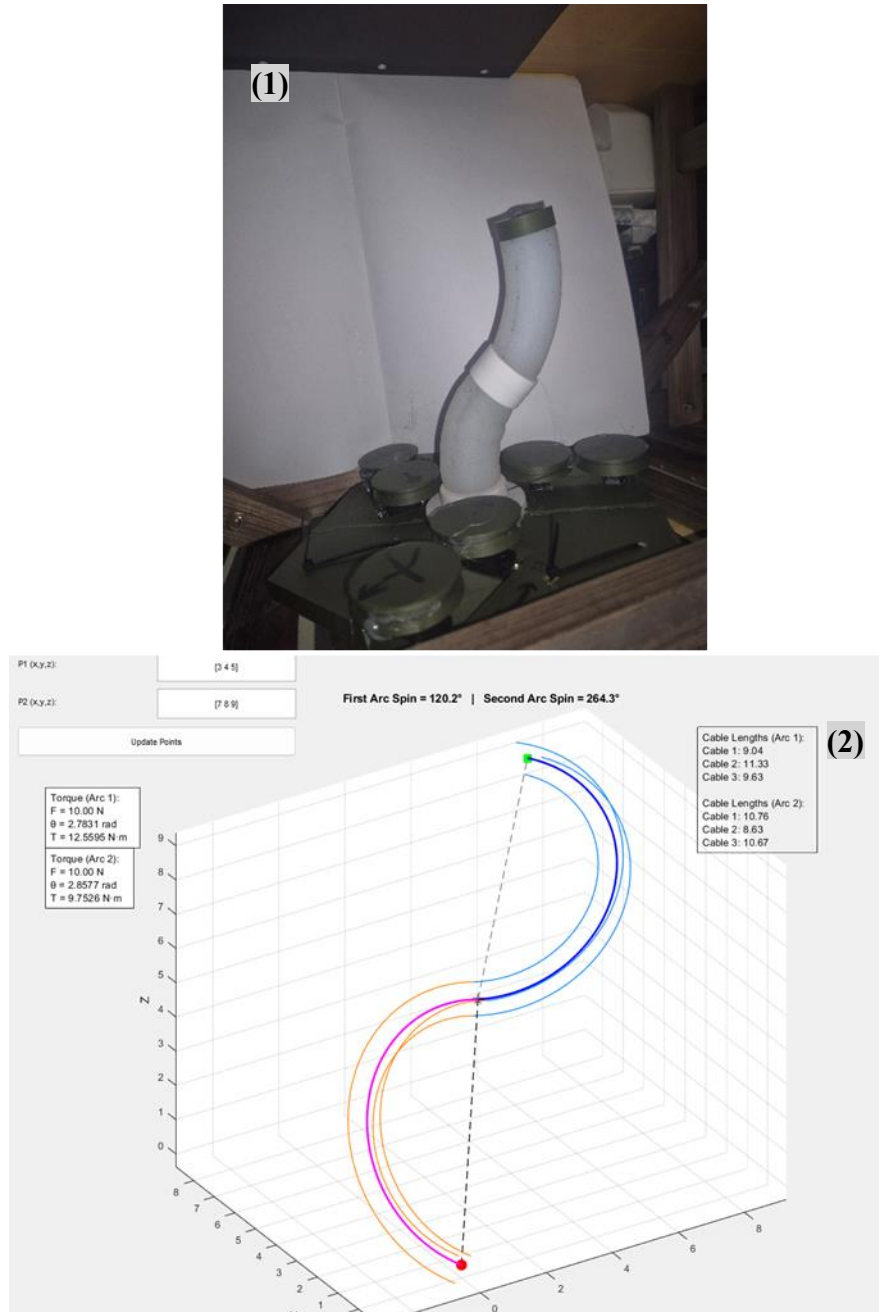


Figure 26 - Actuation of Model Based on Simulation

Friction, therefore, emerged as one of the most critical factors limiting the precision and responsiveness of the system. In the simulation, cable routing was assumed to be ideal, with no internal resistance or material drag. This simplification allowed for consistent motion profiles and the assumption of constant curvature along the length of the

manipulator. In the physical prototype, however, friction between the cables and the inner conduit of the silicone body introduced substantial resistance, which intensified as curvature increased. This resistance not only reduced actuation efficiency but also led to stick-slip phenomena, diminishing control smoothness and introducing latency between commanded input and realised motion. As a result, system responsiveness became increasingly unpredictable, especially during fine manoeuvres or when changing direction.

Moreover, the absence of internal protection around the cables resulted in mechanical abrasion against the surrounding silicone. Over repeated cycles, this direct contact caused visible wear to the silicone body, raising concerns regarding both long-term durability and immediate functional reliability. The lack of internal sleeving also contributed to inconsistent friction along the cable path, making tension and deformation less controllable. These findings indicate that internal sleeving or low-friction conduit materials are essential not only for improving mechanical performance but also for ensuring structural robustness and extending operational lifespan. Simulating these internal interactions more accurately by incorporating variable friction coefficients, material compliance, and dynamic tension loss would provide a more realistic prediction of system behaviour and inform more resilient design choices.

The torque estimation integrated into the simulation framework was predicated upon idealised geometric parameters and the assumption of uniform force transmission throughout the actuator. While this approach yielded foundational insight into the general relationship between actuation force, curvature, and torque generation, it neglected the influence of non-ideal behaviours such as frictional losses, cable tension irregularities, and localised energy dissipation. These factors become especially significant in the 6 DoF models comprising of multiple articulated segments, where minor deviations accumulate, and produce pronounced mechanical discrepancies.

In practice, the torque required to achieve the desired curvature was markedly higher than anticipated, particularly during configurations involving high curvature. Under such conditions, internal resistance due to bending, cable sheath friction, and contact between adjacent layers of the actuator increased substantially. This increase in resistance

introduces a mismatch between the simulated and empirical results, as evidenced in the figure provided. Figure 27 shows the physical configuration of the actuator under

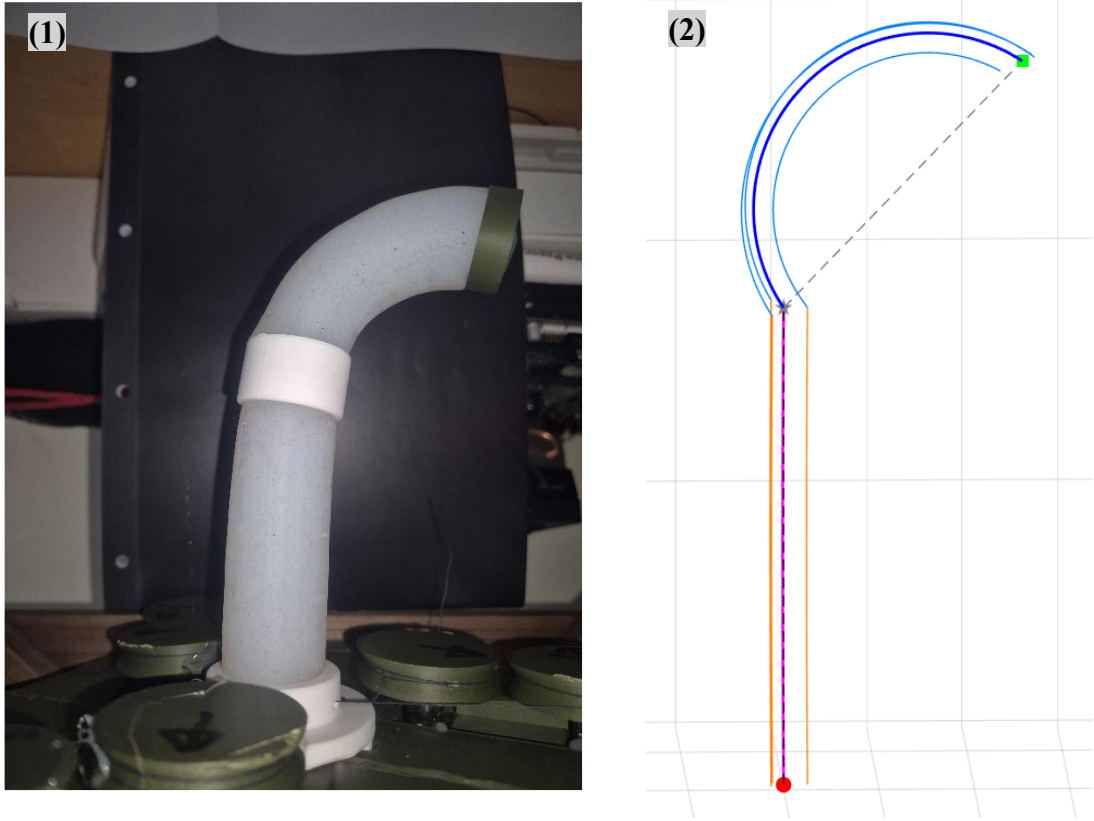


*Figure 27 - Maximum Curvature That Could be Mechanically Achieved with Current Model*

experimental conditions as well as the simulated model. Figure 27 also demonstrates the maximum curvature that could be mechanically achieved with this setup before catastrophic cable failure occurred.

A notable observation in the experimental data is the deviation of the base of the second actuator section from its intended position. This deviation indicates that actuation of the second section introduced reactive forces and torques that influenced the configuration of the first section's end point. This interaction highlights a form of mechanical coupling between segments that was not captured in the original simulation model, largely due to the assumption of perfect decoupling between joints and negligible cable interference. The primary contributing factor to this discrepancy appears to once again, be the excessive internal friction within the cable routing channels.

To address this issue, one viable avenue is to introduce a hybrid compensation strategy



that combines both physical and software-based corrections. Physically, improvements such as those discussed earlier can and should be implemented, however, a purely physical redesign may be insufficient or impractical in some configurations.

Hence, a complementary software-based approach could prove beneficial. This would involve dynamically adjusting the actuation signals of the cables in real time to counteract the effects of unwanted deformation. Such an approach would require the development of more sophisticated torque and friction models that account for non-linearities and segment interactions. These models would need to be supported by experimental data gathered through specifically designed calibration tests. Embedding force sensors at strategic locations within the actuator could allow for the measurement of real-time force transmission and losses. Through this, it would be possible to build a more accurate mapping between input and output parameters, enabling real-time compensation algorithms to function effectively.

### **5.3 Design and Fabrication Reflections**

The fabrication processes for both the 3 DoF and 6 DoF prototypes brought to light a series of practical challenges inherent in the translation of theoretical models into reliable and repeatable physical implementations. The initial proof-of-concept model, constructed with rigid backbones and a spring-based structure, served as an effective platform for preliminary investigations. It allowed for controlled flexibility, facilitated ease of assembly, and enabled early validation of the cable actuation principles and the arc geometry employed in segment articulation.

However, the subsequent transition to a fully soft robotic structure, utilising Ecoflex 00-10 as the primary elastomeric material, introduced a new set of complexities. While this change significantly enhanced compliance and improved anatomical safety for potential biomedical applications, it simultaneously increased the system's sensitivity to cable tension inconsistencies, internal friction within the embedded cable channels, and progressive material fatigue under cyclic loading conditions.

The casting process, although ultimately successful, required meticulous control over several critical parameters. These included the thorough removal of air bubbles during



mixing and pouring, as well as precise alignment of the two-part moulds. In particular, the technique of embedding metal ejector pins into the moulds to create the cable channels proved effective for maintaining consistent channel geometry. However, it also introduced considerable challenges during the demoulding phase. The high adhesion between the silicone and the pins, combined with the thin, solid ribs required for structural support, made it difficult to extract the pins without damaging the part. Instances of tearing or deformation of the silicone body and breakage of the resin-based rib structures were observed. These issues underscore the need for a design revision aimed at reinforcing mechanically vulnerable sections. Substituting resin with a more ductile and impact-resistant material such as aluminium may reduce the likelihood of snapping or cracking during demoulding and repeated use.

To further enhance the robustness and repeatability of the fabrication process, future designs could incorporate mould inserts with integrated channel guides. These would allow the formation of precise cable channels without the need to embed and subsequently extract solid rods from the silicone matrix. By pre-forming the channels during the casting process, the inserts could be withdrawn cleanly and with minimal interaction with the cured elastomer, thereby significantly simplifying demoulding and reducing the risk of mechanical damage to the soft structure.

Selecting a low-friction material for the channel guides would also be advantageous, as it would minimise the coefficient of friction between the inner wall of the channel and the actuation cable. This reduction in friction would not only improve transmission efficiency but also decrease wear on both the channel lining and the cable itself, thereby increasing the overall durability and reliability of the actuator.

Moreover, with a more controlled and lower-friction environment, it would become feasible to use higher-performance actuation cables such as those made from Nitinol, a shape memory alloy composed of nickel and titanium. Nitinol cables are particularly attractive due to their high power-to-weight ratio and unique ability to return to a pre-defined shape upon heating, a behaviour driven by their phase transformation characteristics. This property can be exploited through resistive (ohmic) heating, allowing the cable to autonomously return the actuator to its neutral position without relying solely

on external mechanical retraction via servomotors. This could, in turn, reduce the mechanical load on the motors and improve energy efficiency, especially in cyclic or repetitive applications (Sivaperuman Kalairaj et al., 2019; Hau et al., 2021).

The integration of structural reinforcement materials, such as embedded fibre mesh or high-strength textile layers within the Ecoflex matrix, also presents as a viable method for mitigating excessive deformation and improving the long-term durability of the actuator. Such reinforcement would distribute mechanical loads more evenly and reduce the risk of permanent set or rupture under repeated actuation cycles.

Another critical aspect requiring attention is the precision of the moulding process. Small deviations in mould geometry, whether due to manufacturing tolerances or assembly misalignment, resulted in asymmetrical material distribution and non-uniform cable channel placement. These geometric imperfections not only made the removal of the ejector pins significantly more difficult but also compromised the mechanical symmetry of the final actuator. This, in turn, affected both the repeatability and the predictability of its motion, thereby limiting the fidelity of any simulation-based control strategy. Transitioning to high-precision mould fabrication techniques, such as CNC machining or high-resolution additive manufacturing, could substantially reduce these errors and improve the overall consistency of the soft robotic system.

## 6 Conclusion

This project successfully demonstrated the design, simulation, and partial fabrication of 6 DoF soft robotic manipulator actuated by cables, with a particular focus on addressing the challenges associated with friction and inverse kinematics in surgical applications. Through an extensive literature review, the research highlighted key limitations in existing soft robotic systems, particularly those relating to friction-induced inaccuracies and the complexity of real-time control in cable-driven mechanisms.

A structured methodology was adopted beginning with a 3-DoF spring-based proof-of-concept model, which enabled preliminary validation of the design principles and cable actuation strategy. A geometric and parametric framework was then developed to construct three-dimensional arcs, forming the mathematical foundation for inverse kinematics calculations. This modelling framework was extended into a MATLAB simulation environment that allowed for real-time visualisation, torque estimation, and direct communication with physical hardware via Arduino. This dual arc system enabled spatial representation of a 6-DoF manipulator using constant curvature assumptions, offering insights into actuation strategies and cable routing requirements.

Hardware development involved the design and fabrication of reusable, high-precision moulds for casting silicone segments, with cable channels formed via embedded ejector pins. Although the simulation environment effectively validated the geometric feasibility and control logic of the manipulator, real-world implementation revealed considerable frictional resistance within the cable sheaths. This friction led to diminished control fidelity and hardware limitations such as servo overloading and reduced range of motion. These discrepancies underscored the divergence between idealised simulations and practical constraints, highlighting the necessity for friction modelling, improved material interfaces, and mechanical protection for internal cable routing.

## References

- Arnau Garriga-Casanovas, Shakib, F., Varell Ferrandy and Franco, E. (2024). Hybrid Control of Soft Robotic Manipulator. *Actuators*, 13(7), pp.242–242. doi:<https://doi.org/10.3390/act13070242>.
- Bentley Advanced Materials. (2025). *Ecoflex™ 00-10 - Shore 00-10 Super-Soft, Addition Cure Silicone Rubber*. [online] Available at: <https://www.benam.co.uk/ecoflex-00-10> [Accessed 11 Apr. 2025].
- Blanc, L., Delchambre, A. and Lambert, P. (2017). Flexible Medical Devices: Review of Controllable Stiffness Solutions. *Actuators*, [online] 6(3), p.23. doi:<https://doi.org/10.3390/act6030023>.
- Cheng, S.S., Wang, X. and Desai, J.P. (2017). Design and analysis of a remotely-actuated cable-driven neurosurgical robot. *2021 IEEE/RSJ International Conference on Intelligent Robots and Systems (IROS)*, [online] pp.1685–1690. doi:<https://doi.org/10.1109/iros.2017.8205980>.
- Cosimo Della Santina and Rus, D. (2020). Control Oriented Modeling of Soft Robots: The Polynomial Curvature Case. *IEEE robotics and automation letters*, [online] 5(2), pp.290–298. doi:<https://doi.org/10.1109/lra.2019.2955936>.
- DeLorey, C., Davids, J.D., Cartucho, J., Xu, C., Roddan, A., Nimer, A., Ashrafian, H., Darzi, A., Thompson, A.J., Akhond, S., Runciman, M., Mylonas, G., Giannarou, S. and Avery, J. (2022). A cable-driven soft robotic end-effector actuator for probe-based confocal laser endomicroscopy: Development and preclinical validation. *Translational Biophotonics*, [online] 5(2). doi:<https://doi.org/10.1002/tbio.202200015>.
- Dulęba, I. and Opalka, M. (2013). A comparison of Jacobian-based methods of inverse kinematics for serial robot manipulators. *International Journal of Applied Mathematics and Computer Science*, 23(2), pp.373–382. doi:<https://doi.org/10.2478/amcs-2013-0028>.
- Enyan, M., Bing, Z., Nii, J., Eliasu Issaka, Samuel Leumas Otoo and Michael Freduah Agyemang (2024). Advances in smart materials soft actuators on mechanisms,

fabrication, materials, and multifaceted applications: A review. *Journal of Thermoplastic Composite Materials*, 38(1). doi:<https://doi.org/10.1177/08927057241248028>.

Farid, M.I., Wu, W., Li, G. and Yu, Z. (2024). Research on 3D printing composite material mechanical characterization of robust soft-matter robots. *The International Journal of Advanced Manufacturing Technology*, 133(9-10), pp.4401–4414. doi:<https://doi.org/10.1007/s00170-024-13725-2>.

Gilday, K., Zubak, I., Raabe, A. and Hughes, J. (2024). *From Rigid to Soft Robotic Approaches for Minimally Invasive Neurosurgery*. [online] Paperswithcode.com. Available at: <https://cs.paperswithcode.com/paper/from-rigid-to-soft-robotic-approaches-for> [Accessed 6 Apr. 2025].

Hau, C.T., Gouwanda, D., Gopalai, A.A., Low, C.Y. and Hanapiah, F.A. (2021). Gamification and Control of Nitinol Based Ankle Rehabilitation Robot. *Biomimetics*, [online] 6(3), p.53. doi:<https://doi.org/10.3390/biomimetics6030053>.

Hofstetter, L.W., Hadley, R., Merrill, R., Huy Xuan Pham, Fine, G. and Parker, D.L. (2022). MRI-compatible electromagnetic servomotor for image-guided medical robotics. *Communications Engineering*, [online] 1(1). doi:<https://doi.org/10.1038/s44172-022-00001-y>.

Intuitive Surgical. (2025). *Da Vinci Robotic-Assisted Surgery*. [online] Available at: <https://www.intuitive.com/en-us/patients/da-vinci-robotic-surgery> [Accessed 6 Apr. 2025].

Lanfranco, A.R., Castellanos, A.E., Desai, J.P. and Meyers, W.C. (2004). Robotic Surgery. *Annals of Surgery*, [online] 239(1), pp.14–21. doi:<https://doi.org/10.1097/01.sla.0000103020.19595.7d>.

Li, S., Bai, H., Shepherd, R.K. and Zhao, H. (2019). Bio-inspired Design and Additive Manufacturing of Soft Materials, Machines, Robots, and Haptic Interfaces. *Angewandte Chemie*, [online] 58(33), pp.11182–11204. doi:<https://doi.org/10.1002/anie.201813402>.

Mahboubbeh Keyvanara, Arman Goshtasbi and Kuling, I.A. (2023). A Geometric

Approach towards Inverse Kinematics of Soft Extensible Pneumatic Actuators Intended for Trajectory Tracking. *Sensors*, [online] 23(15), pp.6882–6882. doi:<https://doi.org/10.3390/s23156882>.

Manfredi, L., Yue, L., Zhang, J. and Cuschieri, A. (2018). A 4 DOFs variable stiffness soft module. [online] pp.94–99. doi:<https://doi.org/10.1109/robosoft.2018.8404903>.

Pal, A., He, T. and Wei, W. (2022). *Sample-efficient Model Predictive Control Design of Soft Robotics by Bayesian Optimization*. [online] arXiv.org. Available at: <https://arxiv.org/abs/2210.08780> [Accessed 14 Apr. 2025].

Sivaperuman Kalairaj, M., Banerjee, H., Lim, C.M., Chen, P.-Y. and Ren, H. (2019). Hydrogel-matrix encapsulated Nitinol actuation with self-cooling mechanism. *RSC Advances*, [online] 9(59), pp.34244–34255. doi:<https://doi.org/10.1039/c9ra05360c>.

Song, C., Gao, G., Wang, P. and Wang, H. (2023). Kinematics and Fuzzy Control of Continuum Robot Based on Semiclosed Loop System. In: *2022 2nd International Conference on Robotics, Automation and Artificial Intelligence (RAAI)*. [online] IEEE, pp.43–51. doi:<https://doi.org/10.1109/RAAI56146.2022.10092975>.

Wang, Z., Zi, B., Wang, D., Qian, J., You, W. and Yu, L. (2019). External Force Self-Sensing Based on Cable-Tension Disturbance Observer for Surgical Robot End-Effector. *IEEE Sensors Journal*, [online] 19(13), pp.5274–5284. doi:<https://doi.org/10.1109/jsen.2019.2903776>.

Wild, S., Zeng, T., Mohammad, A., Billingham, J., Dragos Axinte and Dong, X. (2023). Efficient and Scalable Inverse Kinematics for Continuum Robots. *IEEE Robotics and Automation Letters*, [online] 9(1), pp.375–381. doi:<https://doi.org/10.1109/lra.2023.3331291>.

Xu, L. (2017). *MULTI-DIMENSIONAL FIBER OPTIC SENSORS FOR BIOMEDICAL AND SOFT ROBOTIC APPLICATIONS*. [online] Available at: [https://getd.libs.uga.edu/pdfs/xu\\_li\\_201712\\_ms.pdf](https://getd.libs.uga.edu/pdfs/xu_li_201712_ms.pdf) [Accessed 8 Apr. 2025].

Yoon, T., Chai, Y., Jang, Y., Lee, H., Kim, J., Kwon, J., Kim, J. and Choi, S. (2024).

Kinematics-Informed Neural Networks: Enhancing Generalization Performance of Soft Robot Model Identification. *IEEE Robotics and Automation Letters*, [online] 9(4), pp.3068–3075. doi:<https://doi.org/10.1109/lra.2024.3362644>.

Zhang, R., Wang, H., Chen, W., Wang, X. and Pfeifer, R. (2015). Motion analysis and experimental study of a cable-driven soft surgical robot. *2015 IEEE International Conference on Cyber Technology in Automation, Control, and Intelligent Systems (CYBER)*, [online] pp.2085–2090. doi:<https://doi.org/10.1109/cyber.2015.7288270>.

## **Appendix**











### **Appendix A: Code Repository**

The complete codebase associated with this dissertation is accessible through the GitHub repository at:

<https://github.com/SlavicSand/Thesis.git>



# Appendix B: Project Plan

KEY	
	Design Milestone 1 – Have working flexible robot in 3 DoF, should aim for it to have basic functionality and enough to springboard into a 6 DoF robot, around mid to early December
	Deadline 1 - Submit Project Plan (Due 15/10/24)
	Deadline 4 – Presentation (Due 01/05/25)
	Deadline 5 – Submit Final Thesis (Due 21/04/25)
	Miscellaneous Task 1 – Finish literature review, make sure I have a good grasp on what other papers have been written about the topic as well as issues they ran into and possible solutions
	Design Milestone 2 – Have first attempt at flexible robot in 6 DoF, should aim to have a working yet still things to improve at this point by around mid to end of January
	Deadline 2 - Submit Mid-Term Seminar Presentation (Due 20/12/24)
	Design Milestone 3 – Have a final, refined 6 DoF flexible robot, which has had improvements from the first design removing any issues discovered and finished before end of March
	Deadline 3 - Submit Interim Project Report (Due 23/12/24)
	Miscellaneous Task 2 – Complete risk assessment and any other training that would need to be done for use of any equipment (such as 3D printing or testing apparatus)

Ivan Kosko (2481107) - Gantt Chart

